Front. Phys. China, 2010, 5(1): 82–106
DOI 10.1007/s11467-009-0071-1

REVIEW ARTICLE

Brillouin lidar and related basic physics

Da-he LIU (刘大禾)[1,2](✉), **Jin-wei SHI** (石锦卫)[1], **Xu-dong CHEN** (陈旭东)[1], **Min OUYANG** (欧阳敏)[1†], **Wen-ping GONG** (弓文平)[1]

[1] *Applied Optics Beijing Area Major Laboratory, Department of Physics, Beijing Normal University, Beijing 100875, China*
[2] *Key Laboratory of Nondestructive Test (Ministry of Education), Nanchang Hang Kong University, Nanchang 330063, China*
[†] *Now working in School of Information Photoelectric Science & Technology, South China Normal University, Guangzhou 510631, China*
E-mail: dhliu@bnu.edu.cn

Received May 4, 2009; accepted July 20, 2009

The principle of a lidar based on Brillouin scattering is introduced. The basic physics of the Brillouin lidar is discussed. The applications of the Brillouin lidar in remote sensing of the ocean, such as measurement of the sound speed and the bulk viscosity of water and detecting submerged objects are investigated. An actual Brillouin lidar system is developed. Also, several basic problems related to Brillouin lidar are studied in detail. The attenuation coefficient of a pulsed laser beam with high pulsed energy in water is investigated; it is helpful to reveal the propagation property of a laser beam in water. The investigations on the threshold value of SBS are made theoretically and experimentally. Finally, a novel phenomena is investigated experimentally, in which Stimulated Raman scattering can be enhanced by stimulated Brillouin scattering.

Keywords lidar, remote sensing, Brillouin scattering, stimulated Brillouin scattering

PACS numbers 42.68.Wt, 42.79.Qx, 78.35.+c, 42.65.Es

Contents

1 Introduction 82
Part I Brillouin lidar for remote sensing of the ocean 83
2 Principles and techniques of Brillouin lidar 83
2.1 Basic physics of Brillouin scattering 83
2.2 Remote sensing of the ocean based on Brillouin scattering 84
2.3 Actual Brillouin lidar system 86
2.4 Improvement of Brillouin lidar system 88
2.5 Brillouin lidar system based on pumping amplifying effect 89
Part II Basic problems of stimulated Brillouin scattering related to Brillouin lidar 92
3 Attenuation of powerful laser beam in water 92
3.1 Background 92
3.2 Experiments and basic considerations 93
3.3 Experimental results 93
3.4 Analysis and discussion 94
3.5 Conclusion 96
4 Threshold value of stimulated Brillouin scattering 96
4.1 Background 96
4.2 New method for measuring threshold value of SBS 96
4.3 Theoretical discussion on threshold value of SBS 97
4.4 Conclusion 100
5 Stimulated Raman scattering enhanced by stimulated Brillouin scattering 100
5.1 Background 100
5.2 Experiments 101
5.3 Experimental results and discussion 101
5.4 Conclusion 105
Acknowledgements 105
References 105

1 Introduction

In the past three decades, the lidar system based on Brillouin scattering for remote sensing of the ocean has attracted attention [1–8] because of its special properties and high precision. Current authors have made lots of efforts in developing a Brillouin lidar [9–15]. Recently, researchers have greatly improved the characteristics of the Brillouin lidar [16–18] by using stimulated Brillouin

scattering (SBS). In this work, several basic problems were encountered, such as, the attenuation and propagation of powered laser beam in water, the threshold value of SBS, the relationship between SBS and stimulated Raman scattering (SRS), etc., which influence significantly the characteristics of the Brillouin lidar. Therefore, understanding clearly these mentioned fundamental problems has become important in Brillouin lidar. On the other hand, SBS [19–21] is an important topic in the study of non-linear optics. The studies in this area will be helpful for deeply understanding the physical mechanism of powered laser beams. In this article, several problems related to SBS are studied in detail. In Section 2, the attenuation and propagation of a powered laser beam in water are discussed. The effect of SBS on the attenuation of a laser beam in water is studied experimentally. Based on this study, a new method for accurately measuring the threshold value of SBS is suggested. In Section 3, the theoretical threshold value of SBS is deducted rigorously without any empirical assumption; the threshold values of steady state and transient SBS are obtained theoretically. In Section 4, a novel experimental phenomenon in which backward SRS (BSRS) can be enhanced by SBS is reported. Further, this phenomenon is discussed and analyzed in detail.

Part I Brillouin lidar for remote sensing of the ocean

2 Concepts and techniques in Brillouin lidar

2.1 Basic physics of Brillouin scattering

The physical process responsible for Brillouin scattering is the fluctuation in density and concentration. The density fluctuations are composed of two parts. One part is the isentropic pressure fluctuations (phonons) which are propagating in all directions in the water with a velocity $V_{\rm S}$, and the other part is due to the isobaric entropy fluctuations which are frozen and do not propagate. The former is the source of Brillouin scattering. We denote the wave vector of the phonons by $\boldsymbol{q}$, where $|\boldsymbol{q}| = 2\pi/\lambda_{\rm S} = 2\pi\Omega/V_{\rm S}$, $\lambda_{\rm S}, V_{\rm S}$ and Ω are the wavelength, speed and frequency, respectively, of the sound wave.

Consider a fluid of refractive index n that is irradiated by a parallel light beam with wave vector $\boldsymbol{k}$, where $|\boldsymbol{k}| = 2\pi n/\lambda$ and λ is the vacuum wavelength. If the scattered light in the direction of the scattered wave vector $\boldsymbol{k}'$ is observed, then a maximum in the intensity will occur when the wave vectors of the elastic wave $\boldsymbol{q}$, together with the wave vectors $\boldsymbol{k}$ and $\boldsymbol{k}'$ satisfy the Bragg condition (see Fig. 1):

$$\boldsymbol{k}' = \boldsymbol{k} \pm \boldsymbol{q} \tag{2-1}$$

Of course, this is just a statement of the conservation of momentum, the incident wave $\boldsymbol{k}$ either gains or loses momentum from the elastic wave $\boldsymbol{q}$ to produce the scattered wave $\boldsymbol{k}'$. A direct consequence is that for a given wavelength and direction of the incident wave, there is only one wavelength and direction of propagation of the sound that will give rise to a scattered wave in a particular observation direction. Using Eq. (2-1) and the fact that $|\boldsymbol{k}| \approx |\boldsymbol{k}'|$, we have

$$\begin{aligned} q^2 &= |\boldsymbol{k} - \boldsymbol{k}'|^2 = k'^2 + k^2 - 2\boldsymbol{k}\cdot\boldsymbol{k}' \\ &\approx 2k^2(1-\cos\theta) = 4k^2\sin^2\frac{\theta}{2} \end{aligned} \tag{2-2}$$

Here, θ is scattering angle with respect to the direction of the laser beam. Finally, we get

$$q = \frac{4\pi n}{\lambda}\sin\frac{\theta}{2} \tag{2-3}$$

Since the electromagnetic wave is scattering off a moving sound wave, the frequency of the scattered wave will be Doppler shifted. The component of sound velocity in the observation direction $\boldsymbol{k}'$ is $V_{\rm S}\sin(\theta/2)$, and the image of the incident light source moves at twice that speed.

$$V = 2V_{\rm S}\sin\frac{\theta}{2} \tag{2-4}$$

The resulting Brillouin frequency shift $\nu_{\rm B}$, due to the Doppler effect is then

$$\nu_{\rm B} = \pm V\frac{\nu}{c/n} = \pm V\frac{n}{\lambda} \tag{2-5}$$

the scattered wave is both "red" and "blue" Doppler shifted relative to the incident wave. From Eqs. (2-4) and (2-5), we obtain the Brillouin shift

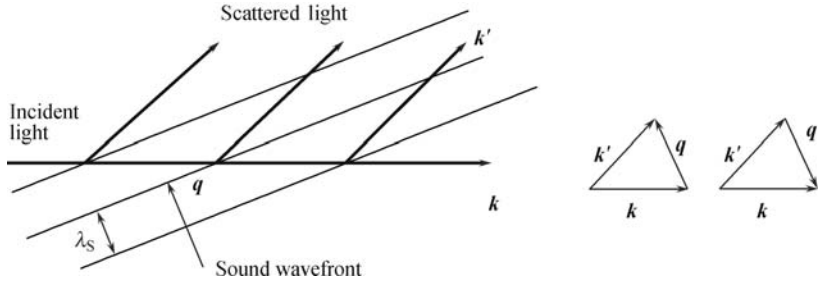

Fig. 1 schematic of the scattering of an incident electromagnetic wave from an elastic wave. $\boldsymbol{k}$, $\boldsymbol{k}'$, and $\boldsymbol{q}$ are wave vectors of incident, scattered and sound wave, respectively.

$$\nu_{\mathrm{B}} = \pm\frac{2n}{\lambda}V_{\mathrm{S}}\sin\frac{\theta}{2} \tag{2-6}$$

Comparing Eqs. (2-3) and (2-6), and using the fact that $q = 2\pi\Omega/V_{\mathrm{S}}$, we find $\nu_{\mathrm{B}} \equiv \Omega$, thus the Brillouin shift is precisely the frequency of the sound wave which satisfies the Bragg condition. Substituting the following typical parameters in Eq. (2-6): $\theta = \pi$ (backscattering), $\lambda = 532$ nm, $V_S = 1500$ m/s, $n = 1.33$, we find $\nu_{\mathrm{B}} = 7.5$ GHz. Such a small shift imposes stringent requirements on measurement techniques that can be used to determine it to sufficient accuracy. Figure 2 shows an idealized Brillouin spectrum. The FWHM of the Brillouin lines (due to acoustic absorption/attenuation) is $\Gamma_{\mathrm{B}} = 0.5$ GHz at 20°C.

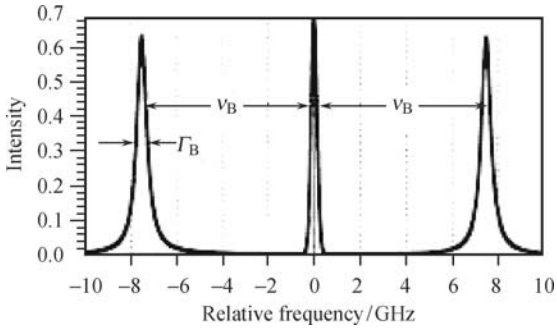

Fig. 2 Idealized spectrum of the Brillouin lines. The two Lorentzians are centered at $\pm\nu_{\mathrm{B}}$, their FWHM is $\Gamma_{\mathrm{B}} = 0.5$ GHz, and they are normalized to unit integrated intensity. A central Rayleigh peak due to elastic scattering is also shown.

The Brillouin width Γ_{B} is also very important for the spectrum of Brillouin scattering. Through some deductions, we obtain [14]

$$\Gamma_{\mathrm{B}} = \frac{1}{\rho}\left[\frac{4}{3}\eta_{\mathrm{s}} + \eta_{\mathrm{b}} + \frac{\kappa}{C_P}(\gamma - 1)\right]q^2 \tag{2-7}$$

where, η_{s} is shear viscosity, η_{b} is bulk viscosity, and κ is the thermal conductivity of the liquid, $q = \dfrac{4\pi n}{\lambda}\sin(\theta/2)$, $\gamma = \dfrac{C_P}{C_V}$. For water, the third term at the right side of the equation is usually two orders of magnitude smaller than the first or the second term, so we have

$$\Gamma_{\mathrm{B}} = \frac{1}{\rho}\left(\frac{4}{3}\eta_{\mathrm{s}} + \eta_{\mathrm{b}}\right)q^2 = \frac{1}{\rho}\left(\frac{4}{3}\eta_{\mathrm{s}} + \eta_{\mathrm{b}}\right)\frac{4\pi^2\nu_{\mathrm{B}}^2}{V_{\mathrm{S}}^2} \tag{2-8}$$

2.2 Remote sensing of the ocean based on Brillouin scattering

2.2.1 Measurement of sound speed of water [15]

From Eq. (2-6), the sound speed of the water can be measured by measuring the Brillouin shift. Figure 3 shows the optical layout. An injection seeded Q-switched Nd: YAG laser was employed as the source. It operates in a single longitudinal mode with a bandwidth of 90 MHz and provides 300 mJ at 532 nm with a repetition rate of 20 Hz, the pulse width is 10 ns. A horn shaped water cell was used to minimize back reflection. The water is circulated through a constant temperature bath that provides an adjustable temperature setting between 0°C and 50°C. The horn was wrapped with fiberglass insulation in order to efficiently cool and stabilize its temperature. The laser used was a scanning Fabry–Perot (Burleigh RC-110), driven by a Burleigh RG-93 ramp generator. The F–P consists of two flat mirrors with a reflectivity of 99.5% and its free spectral range is 18.54 GHz. The photomultiplier tube used was a Hamamatsu R446 operating in the analog mode. The signal is integrated and averaged over 10 laser shots by a gated integrator and boxcar averager (Stanford Research System SR-250). Backscattered light is collected at an angle of 170° to the laser beam direction. The critical point for obtaining good frequency discrimination is to provide a very well col-

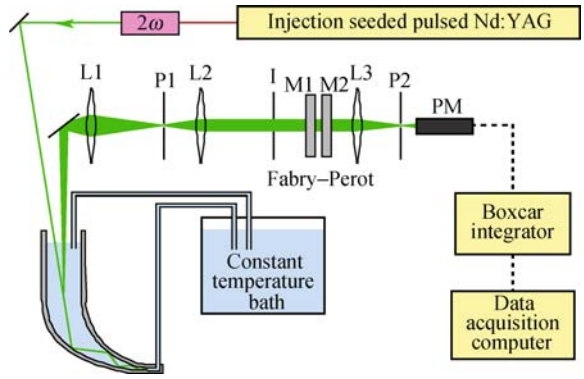

Fig. 3 Schematic for the Brillouin spectrum measurement. L1, L2, and L3 are biconvex lenses with focal lengths 50 cm, 20 cm and 8 cm, respectively. P1 is a 15 μm diameter pinhole, I is an iris, P2 is a 1 mm diameter pinhole, 2 ω is a second harmonic generating crystal, M1, M2 are mirrors, PM is a photomultiplier tube. The horn shaped water cell is wrapped with fiber glass insulation. The constant temperature bath maintains the water in the cell at a constant temperature that can be set from 0°C to 30°C.

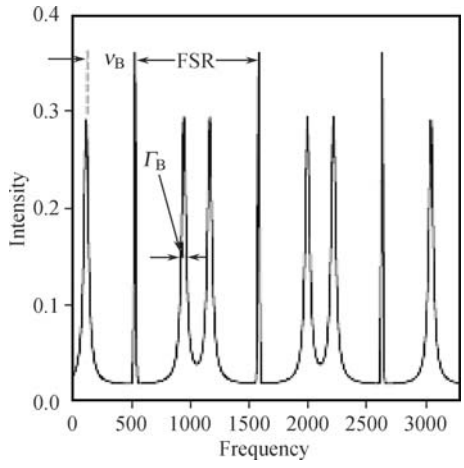

Fig. 4 Fitting result of averaged data. The result is obtained by a mixed function of Gaussians and Lorentzians, where FSR is the free spectral range of the Fabry–Perot interferometer used, ν_{B} is the Brillouin shift, and Γ_{B} is the Brillouin linewidth.

limated beam to the input of the Fabry–Perot. Figure 4 shows the measured spectrum of Brillouin scattering in water, the curve is the fitting result of six groups of measured data.

The measured sound speed of water using Brillouin scattering is given in Fig. 5. In the figure, S is the salinity of the water. These results were compared with the measured data by classical method, the maximum error is 13 m/s, the minimum error is 0.1 m/s, all relative deviations are less than 0.9% related to the classical measurements.

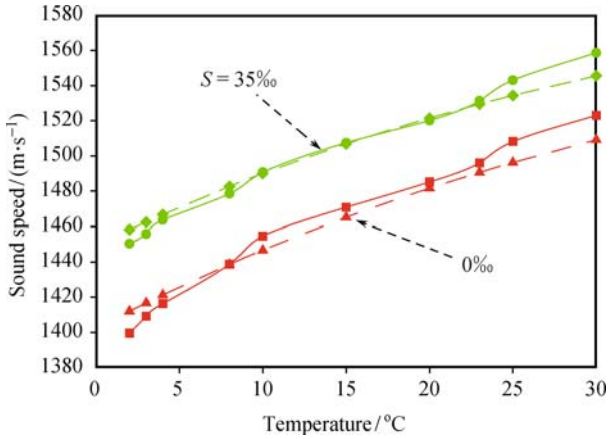

Fig. 5 Measured sound speed in water by Brillouin scattering at different temperatures. The solid lines represent results obtained by Brillouin scattering, the dashed line represent the results measured by classical method.

2.2.2 *Measurement of bulk viscosity of water [14]*

From Eqs. (2-2)–(2-8), we have

$$\eta_{\mathrm{b}} = \frac{\rho v^2 \Gamma_{\mathrm{B}}}{4\pi^2 \nu_{\mathrm{B}}^2} - \frac{4}{3}\eta_{\mathrm{s}} \tag{2-9}$$

There are many databases of the shear viscosity η_{s} of water; therefore, the bulk viscosity of water can be measured by measuring the Brillouin shift and Brillouin line width. Figure 6 shows measured bulk viscosity of water using the set-up geometry shown in Fig. 3. (a) Brillouin line width and (b) shows the measured bulk viscosity based on Eqs. (2-2)–(2-9).

In the same principle, the temperature and salinity of water can also be measured.

2.2.3 *Detecting submerged object [11]*

Briefly, a laser fires pulses into water, the backscattered return signal is recorded as a function of the return time, which is in a one-to-one correspondence with the depth of the signal return. The frequency spectrum of the backscattered light consists of an elastic central peak at the laser frequency (Rayleigh line) and two inelastically scattered Brillouin components related to both "red" and "blue" Doppler shift (see Fig. 2). It is known that Brillouin scattering will occur in water. On the other hand, when a light beam in water is incident on a submerged object, Brillouin scattering will disappear because there is no water at the position where the object locates. In this case, the components of the Brillouin lines will vanish in the returned scattering signal. Thus, if the Brillouin lines do not appear in the spectrum, it means that there must be a submerged object. Figure 7 shows the experimental results using the set-up geometry shown in Fig. 3. During experiments, the scanning time was 10 minutes for getting enough sampling since the repetition rate of the laser used was only 10 Hz. The object was located at a depth of 10 cm just below the water surface.

It can be seen that the spectra with and without submerged object are obviously different, when the object exists the Brillouin scattering disappears. It should be pointed out that, the piece of aluminum in our experiments was milled using milling machine so its surface was leveled up. In Fig. 7 (b) and (c), although the surface reflectivity of aluminum and wood are quite different the structures of the measured spectra are the same.

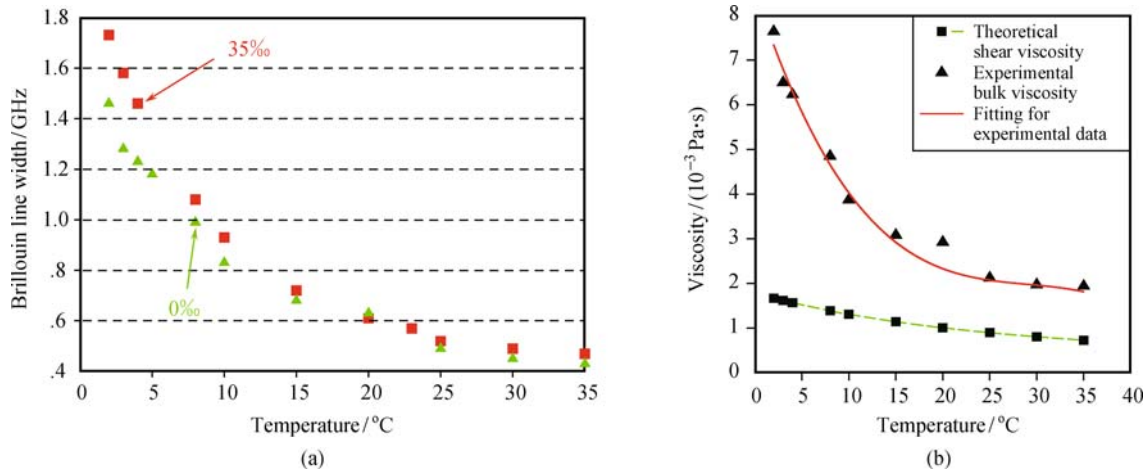

Fig. 6 Measured results of the Brillouin shift and the Brillouin linewidth in water for different temperatures and salinities. **(a)** The measured Brillouin shift at different temperatures. **(b)** The measured Brillouin linewidth at different temperatures. Triangles, the results for fresh water $S = 0$ ‰; squares, the results for water of salinity $S = 35$ ‰.

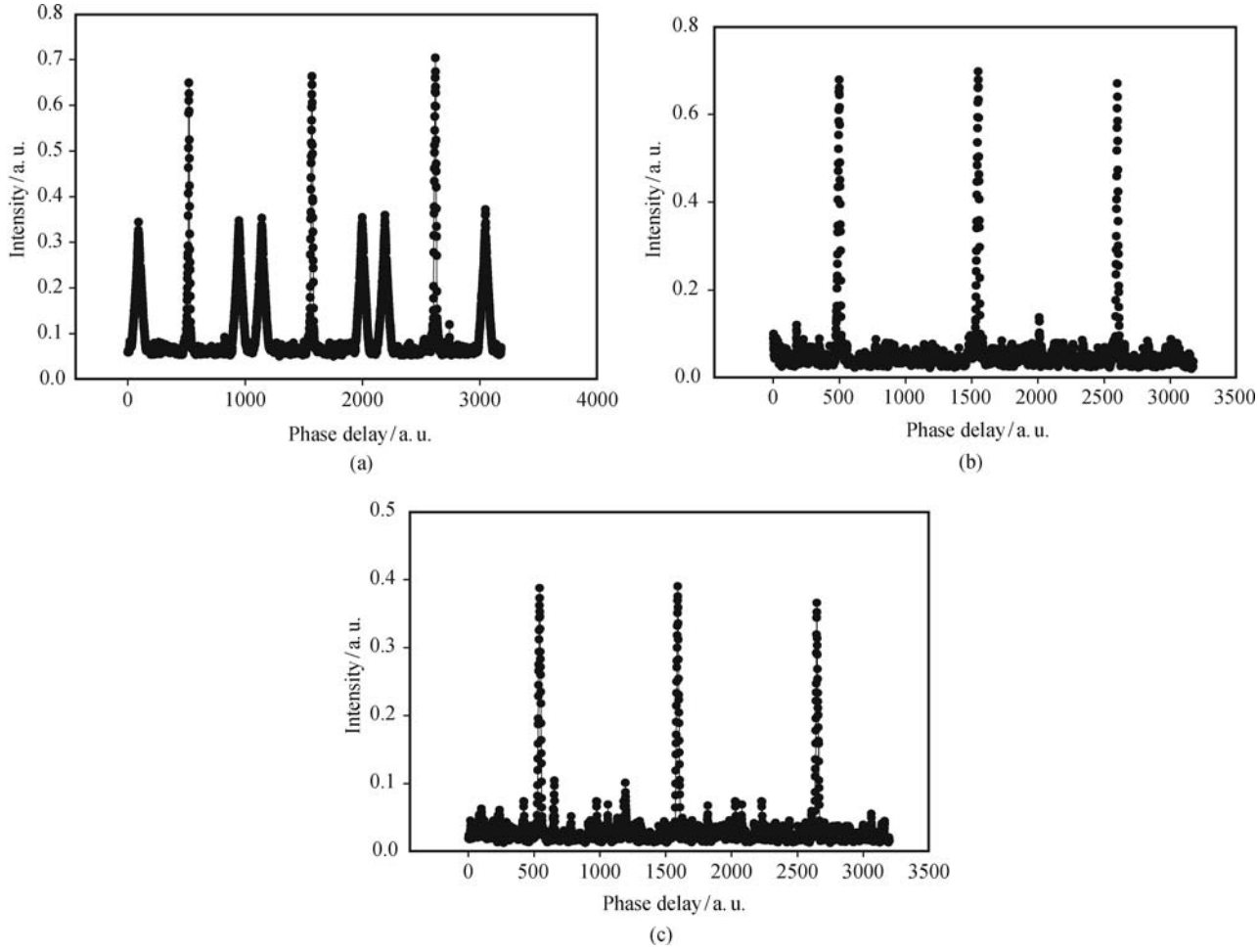

Fig. 7 Laboratory measured spectra of water with and without submerged object respectively. **(a)** Without object; **(b)** With object (a piece of aluminum); **(c)** With object (a piece of wood).

It means that the detection of submerged objects using Brillouin scattering is not sensitive to the surface reflectivity of the detected object.

2.3 Actual Brillouin lidar system

2.3.1 Configuration of the lidar system

Figure 8 shows the configuration of our lidar system in which an F–P etalon and an intensifier CCD (ICCD) camera with gate mode were used as real time detector and image recorder, respectively. The laser used was an injection seeded pulsed Nd:YAG laser (Continnum Powerlite Precision 8000) with line width of 90 MHz, pulse width of 8 ns and repetition rate of 10 Hz, and the pulse energy of the laser beam is 600 mJ. The ICCD used was an ICCD camera (Princeton Instruments PI-MAX 1024B), with minimum gate width of 2 ns and the pixel size of 26 μm. The F–P etalon used was a solid etalon made of quartz with a free spectral range of $FSR = 22.4$ GHz. The pulse generator used was a DG-535 (Stanford Research System).

The polarization of the output laser beam is horizontal. It penetrates the polarizer with very low energy loss,

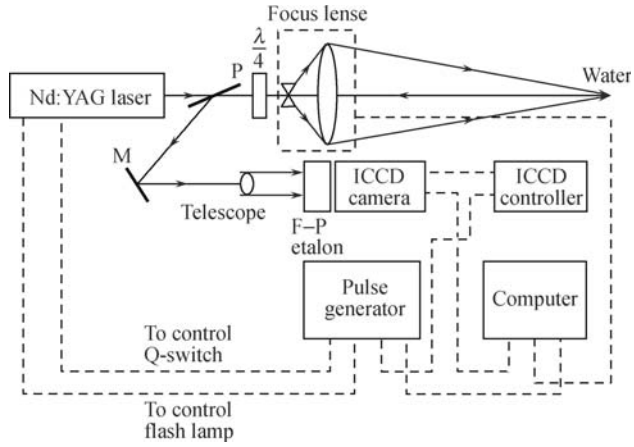

Fig. 8 Configuration of Brillouin lidar system. P is polarizer, $\lambda/4$ is quarter wave plate. The solid lines represent the connections of light, dashed lines represent electronic connections.

and after passing through the $\lambda/4$ plate it becomes R-circle polarization. The laser beam can be focused at different depths in water by the focusing system. The focus depth can be controlled by adjusting the space between the two lenses controlled by a computer. In the range close to the focus point, the energy density of the laser is high enough so that Stimulated Brillouin scattering

(SBS) will happen. SBS is very helpful in increasing the detection depth and in improving the depth resolution of the measurement [6], it will be discussed later. The back scattered SBS light passes through the $\lambda/4$ plate again, its polarization becomes vertical, and it is reflected by the polarizer P without energy loss. The back scattered SBS light was collimated by the telescope, then incidents on the F–P etalon. The spectrum of Brillouin scattering formed by the F–P etalon was recorded by the ICCD camera. With this lidar system a spectrum generated by a single laser shot can be recorded.

2.3.2 Experimental results

The measurements were carried out in an outdoor 55-m long horizontal water tank in Nanchang City, at an outdoor temperature of 4°C–20°C. The salinity of the water was 0 ‰.

(1) Measurements of sound speed in water

Brillouin shift should be measured first in order to determine sound speed in water. One of the recorded spectrum of Brillouin scattering in water is shown in Fig. 9, which shows that, each order in the spectrum includes two rings, the outer one represents Rayleigh scattering, and the inner represents Brillouin scattering. It should be pointed out that there is only Stokes line and no anti-Stokes line in the spectrum, which is the typical phenomena of stimulated Brillouin scattering. The Brillouin shift can be determined by

$$\Delta\nu_{\mathrm{B}} = \frac{r_{j-1}^2 - r_{j-1}'^2}{r_j^2 - r_{j-1}^2}\mathrm{FSR} \tag{2-10}$$

where, r_j, r_{j-1} are the radius of jth and $(j-1)$th order of the Rayleigh peak respectively, and r'_{j-1} is radius of $(j-1)$th Brillouin peak. Their values equal to 26 μm multiplied by the pixel number which is included by a ring (see Fig. 2). The deduction of the formula (2-10) can be easily finished based on Eq. (50) of Chapter 6 in "Principles of Optics" (7th edition) written by Born and Wolf. Table 1 gives the measured Brillouin shift and sound speed in water at several temperatures using the configuration shown in Fig. 8. The sound speed at different depths in water can be determined by the time delay of the returned signal. In this way, the profile of sound speed in water with depth can be obtained.

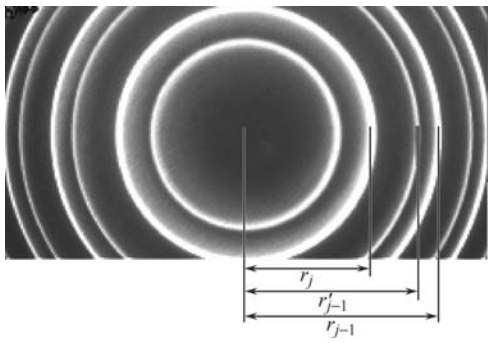

Fig. 9 Measured spectrum of Brillouin scattering in water.

Table 1 Measured sound speed in water at different temperatures

Day	Temperature/°C	$\Delta\nu_{\mathrm{B}}$/Hz	$V_{\mathrm{S}}/(\mathrm{m\cdot s^{-1}})$
1	4	7.119	1423.8
2	8	7.227	1445.4
3	10	7.293	1458.6
4	12	7.324	1464.8
5	15	7.349	1469.8
6	18	7.404	1480.8
7	20	7.433	1486.8
8	23	7.476	1495.2

(2) Source of error in the system

Comparing the above data with the results given in Ref. [15], there is a little difference between the two measurements. Since the principles of the two systems are essentially the same, the factor causing the error must lie in the system itself. The measuring uncertainty of sound speed is expressed as [15]:

$$\delta V_{\mathrm{S}} = \sqrt{\left(\frac{\partial V_{\mathrm{S}}}{\partial S}\right)^2 (\delta S)^2 + \left(\frac{\partial V_{\mathrm{S}}}{\partial \nu_V}\right)^2 (\delta\nu_{\mathrm{B}})^2} \tag{2-11}$$

When the salinity of water is fixed, the uncertainty is related directly to the accuracy of the measurement of Brillouin shift. However, another factor must be taken into consideration in the suggested system using ICCD camera. The pixel size of the CCD would have obvious influence on the error. The output of a pixel of a CCD is formed by the whole pixel although a peak in the scattered spectrum may only cover a small fraction of the pixel. Therefore, the larger the pixel size the larger the measuring error. The pixel size of the CCD we used is 26 μm, it will result in an extra measuring error of Brillouin shift. Therefore, an ICCD camera with smaller pixel size is preferable for reducing measuring error. Comparing the results of Table 1 and Ref. [15], the difference between them just comes from the pixel size of the CCD used. If a CCD camera with smaller pixel size is used, more accurate measurement could be obtained.

(3) Measurements of bulk viscosity of water

According to Ref. [14], the bulk viscosity of water is determined by the Brillouin line width. The Brillouin line width can also be measured by the above suggested system. However, because the value of the Brillouin line width (about 500 MHz) is much less than the value of the Brillouin shift (about 7.5 GHz), using the ICCD camera with the pixel size of 26 μm, the measured results were unsatisfactory. Therefore, the measured results are not shown here. If an ICCD camera with small pixel size is used, the measured results will be improved greatly.

(4) Experiments for detecting submerged objects

According to the principle in Section 2.2, whether an object exists in water can be recognized by the spectrum of Brillouin scattering in water, since no Brillouin scattering would occur at the location where water is displaced by an object. In our experiments, the submerged object was a piece of aluminum packed by black cloth. The detected distance was 40 meters. Figure 10 shows the experimental results. It can be seen that detecting a submerged object by Brillouin scattering is very easy. If each order in the measured spectrum contains two rings, it means that there is no submerged object. If each order in the measured spectrum has only a single ring, it means that there is an object in the water.

2.4 Improvement of Brillouin lidar system

Using our lidar system shown in Fig. 8, we carried out measurements in a 40 m long water tank. When the laser beam was focused at the distance of 15 m; spectra at 3 m and at the focused point (15 m) were recorded respectively. Figure 11 gives the two spectra. It can be seen clearly that in the spectrum of spontaneous scattering both Stokes and anti-Stokes components are observed. However, in the spectrum of stimulated scattering, only the Stokes component can be observed. From Fig. 11 it

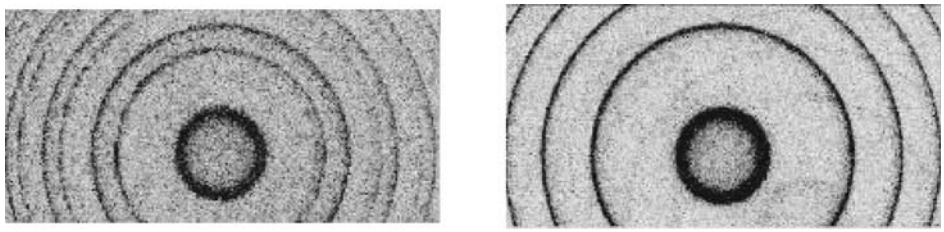

Fig. 10 Experimental results for detecting submerged object in terms of Brillouin scattering. **(a)** Without submerged object; **(b)** With submerged object.

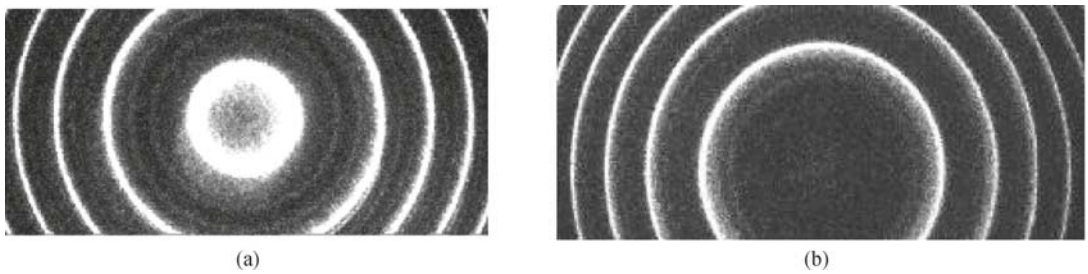

Fig. 11 Measured spectra of spontaneous at 3 m and stimulated Brillouin scattering at 15 m depth in water. **(a)** Spontaneous Brillouin scattering recorded at 3 m depth. SNR = 2.4; **(b)** Stimulated Brillouin scattering recorded at 15 m depth. SNR = 2.5.

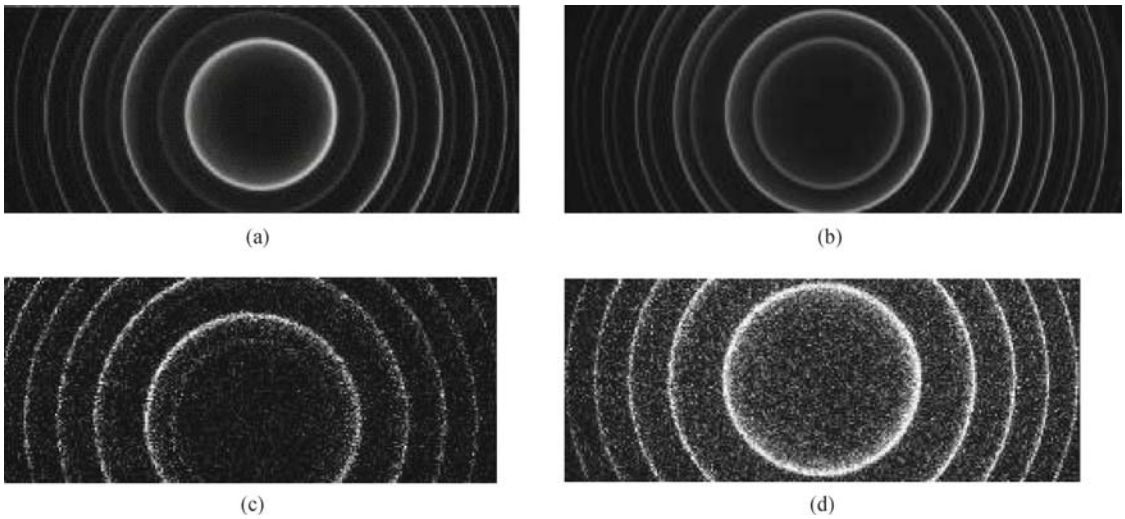

Fig. 12 Measured spectra of stimulated Brillouin scattering at different depths in water using focus lens with diameter of 15 cm. **(a)** 3 meters depth. SNR = 136; **(b)** 9 meters depth. SNR = 28; **(c)** 18 meters depth. SNR = 2.6; **(d)** 22 meters depth. SNR < 1.2.

can be seen that the signal-to-noise ratio (SNR) at 15 m depth for stimulated scattering is almost the same as that at 3 m depth for spontaneous scattering (with SNR = 2.4), where, the SNR is defined as the ratio of the signal intensity and the back noise of the ICCD detector (including the dark noise of CCD and back noise of detecting).

It means that much deeper depth can be detected by stimulated scattering with the accuracy at a small depth detected by spontaneous scattering. Spectra of stimulated Brillouin scattering at different depths were measured at those depths. The results are shown in Fig. 12. For each interference order, there are two circles, the inner is the Brillouin component and the outer is the Rayleigh component. As we can see, the signal-to-noise ratio of the Brillouin scattering is increased so much. For a depth of 22 m, the backscattered signal is too weak to be detected. It should be pointed out that the detected depth is related to the diameter of the focusing converge lens.

Also, we can see that for the depth of 9 m, the energy of the Brillouin component is very high; even, the energy of the Brillouin component is much higher than the energy of the Rayleigh component at the lower depths. The results given in Fig. 12 were obtained using a focusing lens with a diameter of 15 cm. When another lens with a diameter of 30 cm was used, the stimulated scattered spectrum at the same depth of 22 m was measured too, and the result is shown in Fig. 13. The Stokes component of the stimulated Brillouin scattering can still be seen, though it is not very clear.

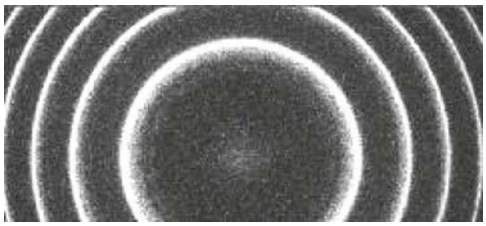

Fig. 13 Measured spectra of stimulated Brillouin scattering at 22 m depths using focus lens with diameter of 30 cm. SNR = 2.1.

Another advantage of stimulated Brillouin scattering as used for remote sensing of the ocean is also significant. Generally, when the pulse width of a laser used is 10 ns, the theoretical depth resolution in water is about 1m for a lidar system with spontaneous scattering. However, if the measurement is based on stimulated scattering, the depth resolution in water will be greatly improved. The reason is because stimulated Brillouin scattering happens only when its threshold condition is satisfied. When a divergent laser beam with large cross section area passes through a converging focusing lens, the energy density is concentrated along its propagation more quickly than without a lens. Therefore, the depth range satisfying the threshold condition of stimulated scattering will become very short so that the depth resolution can be improved greatly. In our experiments, when no focusing lens was used, the depth resolution in water is about 160 cm, but when the focusing lens was used, the depth resolution in water becomes as short as 20 cm. As verification, in our experiments, the laser beam was just focused by a lens with the diameter of 30 cm at the object at a depth of 22 m; the spectrum like that shown in Fig. 10(b) was measured. When the object was moved away for 20 cm, the spectrum like that shown in Fig. 10(a) was measured; it means that the depth resolution is 20 cm. Of cause, for the large depth, the focusing point will become longer and the depth resolution will be decrease. In our experiments, when the detected depth was 50 m, the laser beam was focused to a line close to 1 m. In this case, the depth resolution may be about 1 m.

It should be mentioned that the depth resolution is affected by the signal crosstalk from other depths than the depth of interest, and is related to the gate width of the detector. In our proposed system, we chose the minimum gate width (2 ns) of the ICCD system we used. In this case, only the signals in a short range of the depth can be detected by the ICCD; the signals from other depths cannot be received because the detector is not opened when the signals arrive at the ICCD.

Also, it should be pointed out that, although the submerged object can be detected by this method (see Fig. 10), what kind of object cannot be known. For recognizing the detected object the laser scanning technique must be used practically.

2.5 Brillouin lidar system based on pumping amplifying effect

Stimulated Brillouin scattering (SBS) has distinctive features as compared with spontaneous Brillouin scattering and has been broadly applied in the fields of phase conjugation and pulse width compression. The present authors hold the opinion that SBS could be used for improving lidar. The most effective measure is to amplify the very weak signal of the backscattered SBS, which is almost exhausted after penetrating the surface of the water, especially when the detected depth is very deep or the water is turbid. However, although the dual cell amplification method is usually used in laboratories, it is impractical for field use because it is impossible to build an isolated cell for amplification, since the ocean is practically only a single cell. Moreover, an extra pumping beam is needed for amplifying the seed signal of SBS. In a lidar system or another application, these two beams should be coaxial. The most-used method for coupling the two beams into a single collinear beam is polarization coupling, in which the polarizations of the two beams are orthogonal. However, the two beams with orthogonal polarizations are not coherent, thus amplification cannot

be achieved. Therefore, implementation of amplification of two beams with orthogonal polarizations becomes the key point for further improvement of the lidar system. Recently, the present authors developed a method that gave two coaxially transmitted pulsed beams with orthogonal polarizations possess same polarization during a key moment of time and achieved the amplification of a very weak backscattered SBS signal by the pumping effect. It is described as follows.

The optical layout of the lidar system is shown in Fig. 14. A pulsed Nd:YAG laser produces two beams, a beam with fundamental frequency at 1064 nm wavelength, and another beam with frequency doubling at 532 nm wavelength (beam 1). The beam at 1064 nm was allowed to pass through a frequency-doubling crystal to get another beam also at 532 nm wavelength (beam 2). Beams 1 and 2 are coherent since they are produced by the same oscillator with the same frequency, phase, and polarization. Beam 1 passes through a half-wave plate and is converted from vertical polarization to horizontal polarization and then passes through a polarization coupler, P1, with a transmissivity higher than 90%. Beam 2 remains vertically polarized and is reflected by polarization coupler P1 with reflectivity of 95%. Beams 1 and 2 are coupled into one beam of a pulse series after passing through P1 and are then transmitted coaxially. Each series consists of a pair of orthogonally polarized pulses. Beam 1 is used for exciting SBS in the water, while beam 2 is used to amplify the SBS signal by pumping effect. The laser used in our experiments is an injection seeded pulsed Nd:YAG laser (Continuum Powerlite Precision Plus). Its repetition rate is 10 Hz. The output energy of a single pulse is 1.5 J at 532 nm (beam 1). It gives another simultaneous output at 1064 nm with single pulse energy of 1:3 J, which is converted into a beam with 532 nm and single pulse energy of 650 mJ (beam 2) after passing through a frequency-doubling crystal, SH. The polarization of the backscattered SBS becomes perpendicular to that of the incident beam passing through polarization couple P2, so the SBS signal will be reflected by P2 with a reflectivity of 95%.

Now, the function of the polarization controller is explained in detail as follows. Since SBS has the feature of phase conjugation, it can be amplified when it meets a coherent beam. There can be a time delay between the SBS seeder signal and the pumping beam. This makes the basis of the design of a polarization controller for coaxial pulse series with orthogonal polarizations.

(1) Basic principles

The polarization controller consists of an electro–optic crystal and a driver. Let the coaxial beam consist of two pulses coming from the polarization coupler with orthogonal polarizations incident on the polarization controller. The two pulses reach the electro–optic crystal at different times sequentially. The axis of the crystal is vertical when high voltage is not applied but becomes inclined 45° when high voltage is applied and then functions as a half-wave plate for the next coming beam. Therefore, the t characteristics of birefringence are changed by applying high voltage on the electro–optic crystal or not to control the polarization of the two pulses.

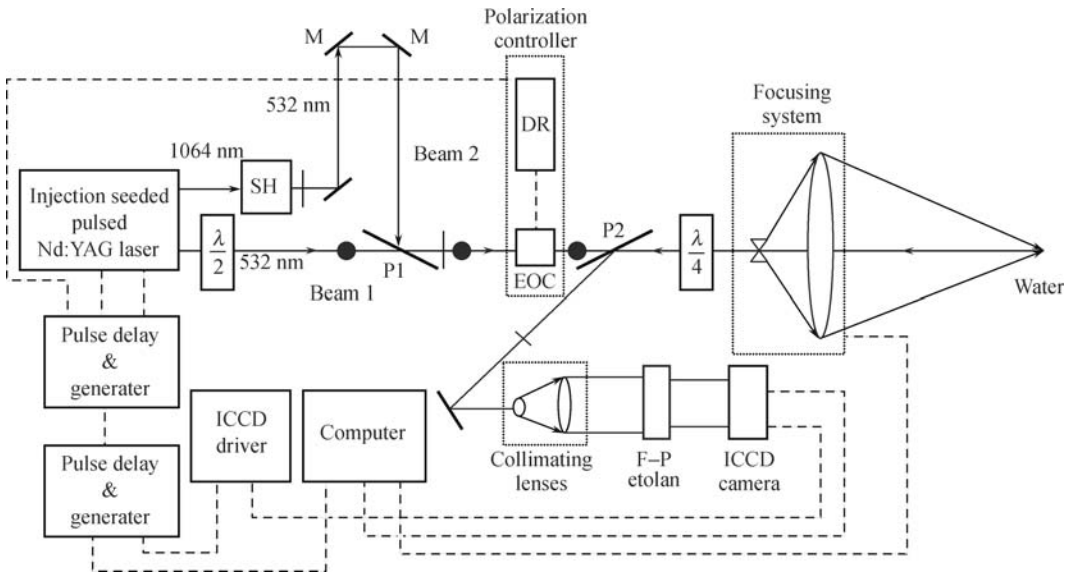

Fig. 14 Experimental set-up geometry. $\lambda/2$ is a half wava plate, $\lambda/4$ is a quarter wave plate; M is mirror; P is polarization coupler; SH is a frequency doubling crystal; EOC is an electro-optic crystal, and DR is the driver of the crystal. The sign "|" represents the polarization perpendicular to the incident plane, and the sign "•" represents the polarization parallel to the incident plane. The incident plane is perpendicular to the paper surface. The solid lines with arrows represent the connections with optical signals. The dashed lines represent the connections with electronic signals.

(2) Method of implementation

In our method, the voltage-increasing mode was used, in which high voltage is not applied on the crystal initially so that the lifetime of the crystal can be prolonged. (The voltage-decreasing mode has higher switching speed and is preferred when a shorter switching time is needed.) Suppose that the pulse width of the laser is 10 ns, the repetition rate of the laser is 10 Hz, and the coaxial beam is composed of two pulses with orthogonal polarizations: the working process of the polarization controller will be as follows:

(i) Two orthogonally polarized beams are coupled into one coaxial beam after passing through the polarization coupler. There is a time delay (>10 ns) between the two pulses. Suppose that the horizontally polarized beam represented by "•" in Fig. 14 arrives first.

(ii) High voltage is not applied to the electro–optic crystal in the initial state. At this time the pulse with "•" polarization (beam 1) will pass through the crystal with very little energy loss, and the pulse width is 10 ns.

(iii) More than 10 ns later (the time delay can be adjusted according to the pulse width of the laser), after the first arriving pulse with "•" polarization has passed. After another certain time delay (it can be adjusted according to the increasing time of the high voltage), the other vertically polarized pulse, represented by "|" in Fig. 14 (beam 2), arrives at the crystal. At this time, high voltage is applied abruptly to the crystal by the driver, the crystal abruptly becomes a half-wave plate, and the axis of the crystal is 45° with respect to the "|" polarization. Thus, the pulse with "|" polarization will pass through the crystal with very little energy loss and the "|" polarization will be changed to "•" polarization.

(iv) Again, more than 10 ns later, after the pulse of beam 2 passes through the crystal, the high voltage on the crystal is cut off abruptly, and the characteristics of birefringence of the crystal returns to the initial state.

(v) After a certain time delay (which is determined by the repetition rate of the laser), the second pair of pulses arrive at the polarization controller sequentially, and the process of 1 through 4 is repeated.

(vi) The above process is repeated continuously. The two orthogonally polarized pulses will have the same polarization in every repeated segment of the whole process.

(vii) The driver of the electro–optic crystal is controlled by a high precision pulse delay and generator to ensure accuracy.

Figure 15 shows an actual polarization controller and chronological sequences of laser pulses and the switching on and off of the high voltage. Figure 15(a) is the polarization controller. In Fig. 15(b), the left and right peaks of the curve starting in the middle of the three on the left are the pulse pair of beam 1 and beam 2, respectively. The wide peak of the curve starting at the bottom left is the high voltage pulse generated by the driver. The curve starting above the other two on the left is the trigger signal output by the laser. The specifications of the polarization controller are as follows: the material of the electro–optic crystal is KD*P, the aperture of the crystal is 15 mm, the working mode is voltage increasing, the half wave voltage is 7000 V, and the width of increasing time is 27 ns. The pulse delay and generator used was a DG 535 (Stanford Research Systems).

Figure 16 shows the profiles of the pulses after passing through the polarization controller. The pulse profiles were detected by a 200 ps detector placed in front of the collimating lenses in Fig. 14 and was recorded by an oscilloscope (Agilent 54832 B). It can be seen that the polarization controller achieved the expected control of the orthogonally polarized coaxial pulse pair.

Because the width of the increasing time of the high voltage pulse is 27 ns, the time delay of the pulse of the beam 2 was adjusted to 27 ns with respect to the pulse of the beam 1, which corresponds to an optical path of 5 m, i.e., the SBS elicited by the pulse of beam 1 will meet the pumping pulse of beam 2 at a distance of 2.5 m in

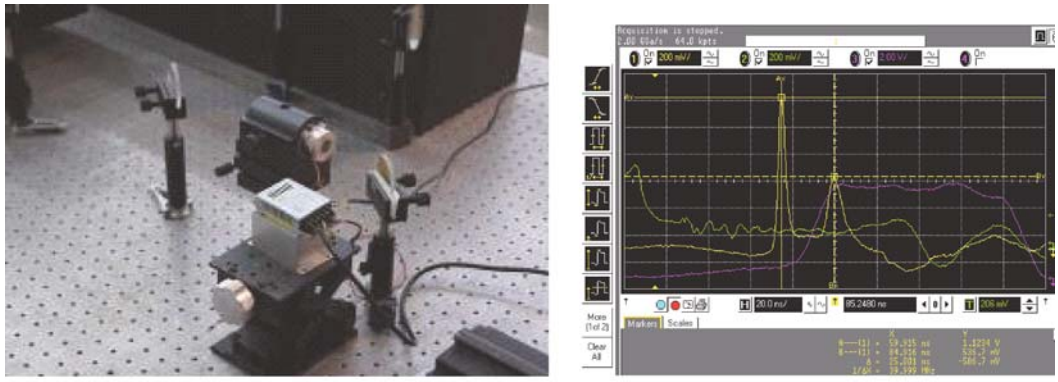

(a) (b)

Fig. 15 Polarization controller and chronological sequences. **(a)** Polarization controller; **(b)** Chronological sequences of laser pulses and the switching on and off of the high voltage. The yellow peaks are the pulse pair of beam 1 and beam 2, respectively. The wide purple peak is the high voltage pulse generated by the driver. The green curve is the trigger signal output by the laser.

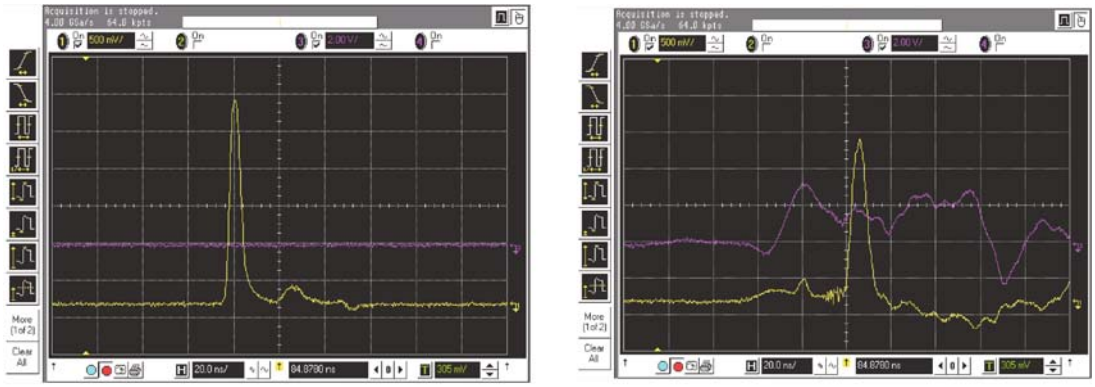

(a) (b)

Fig. 16 Control of the polarizations of the two orthogonally polarized coaxial pulses. **(a)** Without high voltage. The pulse of beam 1 can be detected, the pulse of beam 2 cannot be detected. **(b)** With high voltage. The pulse of beam 2 can be detected, the pulse of beam 1 cannot be detected.

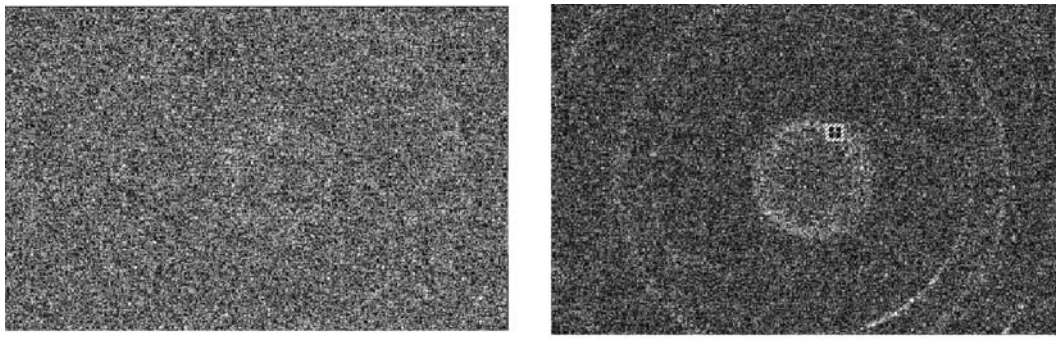

(a) (b)

Fig. 17 Measured spectra with and without pumping amplification. **(a)** Spectrum without amplification by pumping pulse of beam 2. **(b)** Spectrum with amplification by pumping pulse of beam 2. The maximum SNR = 4.7.

its backward travel. At this time, as controlled by the polarization controller, the polarization of beam 2 is the same as that of the SBS signal elicited by beam 1. Therefore, the SBS signal is amplified to the utmost degree, and then its spectrum is obtained clearly with an ICCD camera (Princeton Instruments PI-MAX2 1003) after passing through a Fabry–Perot etalon. Considering that the width of the increasing time of the high voltage pulse is 27 ns and the interaction length is approximately 5 m in the water, hence a 10 m long water tank was chosen for the experiment (see Fig. 14). The attenuation coefficient of the water was 1.3 m^{-1}, which corresponds to an attenuation length of 0.83 m. Figure 17 shows the measured SBS spectra at a depth of 7 m in the water with and without amplification by a pumping beam. The gate width of the ICCD camera was 5 ns. It can be seen that the SBS signal without pumping amplification is extremely weak and that it cannot be detected by the ICCD camera. When pumping amplification was used, owing to the existence of the second pulse of beam 2, the weak SBS signal evoked by the pulse of beam 1 at 7 m depth met the pumping pulse of beam 2 after traveling backward 2.5 m and was amplified significantly with the maximum signal-to-noise ratio of 4.7. The complete scattering spectrum was recorded by the ICCD camera with the same gain.

The above experimental results show that amplification of SBS of two coaxial pulsed laser beams with orthogonal polarization can cause a decided change in the weak SBS signal from undetectable to clearly detected by using the designed polarization controller.

Part II Basic problems of stimulated Brillouin scattering related to Brillouin lidar

3 Attenuation of powerful laser beam in water [22]

3.1 Background

The attenuation of light in water is a matter of broad concern in ocean optics, and it plays a major role in lidar systems used for remote sensing of the ocean. It is influenced by two factors, absorption and scattering. In pure water and in the open ocean, absorption is generally the dominant factor [23]; it is dependent on the wavelength of the light, but for the 532 nm wavelength focused in this study it is considered as a constant. Based on a number of experimental measurements, the value of

the absorption coefficient of pure water at 532 nm is ∼ 0.04–0.05/m [24–26].

For an oceanographic lidar, a pulsed laser is operated at high-power to maximize the penetration depth. But for a Brillouin lidar [3, 4, 13] the pulsed laser must also have a narrow line width. In our recent work a narrow line width, high power laser clearly changed the propagation properties of light in water. Specifically, at sufficiently high laser intensity, stimulated Brillouin scattering (SBS) is observed, and SBS has been used in practical lidar systems [17]. In the presence of SBS, the attenuation coefficient of a pulsed laser in water cannot be considered simply as a constant; it will increase with an increase in laser intensity. This phenomenon is investigated in the following.

3.2 Experiments and basic considerations

The attenuation coefficient for a pulsed laser beam in water was measured at different pulse energies. Figure 18 shows a schematic for the optical layout of our experiments. The laser system is an injection seeded Nd:YAG laser (Continuum Powerlite Precision II 8000) with a line width of 30 GHz and 90 MHz when the seeder is switched on and off, respectively. Its pulse width is 8ns, and its repetition rate is 10 Hz. The 532 nm operating wavelength was produced by frequency doubling. The two detectors were power meters, Coherent FIELDMATE and Newport 1835-C. Measurements were made at different pulse energies; and in order to keep the output characteristics of the laser unchanged, the pulse energy of the laser was adjusted by changing the time delay between oscillator and amplifier. The lengths of the water cells were 0.8, 1.2, 1.6 and 2.0 m, respectively; for comparison, the length corresponding to 8 ns laser pulse is 2.4 m. For simplicity, and also since the attenuation coefficient of light in tap water may be closer to that of the open ocean than distilled water, tap water was used in our experiments. Although tap water typically contains large amounts of dissolved organic matter (DOM), it leads both to absorption and to fluorescence which can be scattered into the detectors. The absorption by DOM will not change during the experiments and is included in the absorption of water. It will not influence our experimental results, as is the case for measurements in the open ocean. The fluorescence is quite weak compared to SBS, and can be observed in all directions; the SBS signal is concentrated in the back scattering. Therefore, the effects of fluorescence by DOM can be neglected.

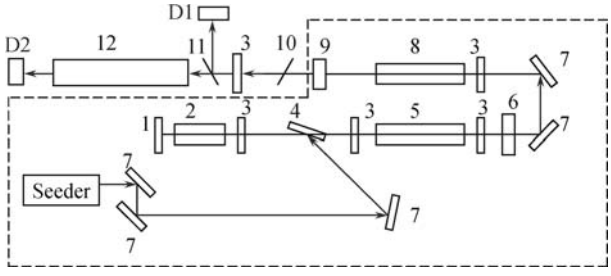

Fig. 18 Optical layout for measuring the attenuation coefficient of a pulsed laser in water. 1. Rear mirror, 2. Pockels cell, 3. 1/4 Wave plate, 4. Dielectric polarizer, 5. Oscillator rod, 6. Output coupler, 7. IR mirror, 8. Amplifier rod, 9. SHG, 10. Polarizer, 11. Beam splitter, 12. Water cell. D1 is detector 1 and D2 is detector 2.

The measurement approach is described as follows. First, the laser beam passes through the empty cell without any water, and I_1 and I_2 are recorded by detectors 1 and 2, respectively. If the beam splitter ratio is k_1 and the attenuation by the two end windows of the cell is k_2, then, I_2 can be expressed as:

$$I_2 = I_1 k_1 k_2^2 T_1^4 \tag{3-1}$$

where, T_1 is the transmission coefficient at a glass-air interface. Next, the cell is filled with water while keeping the layout unchanged, and the same measurements were repeated. The new data, I_1' and I_2', detected by detectors 1 and 2, respectively, were recorded. Assuming that the average attenuation coefficient of light in the water is γ and the length of the cell is l, then, I_2' can be expressed as:

$$I_2' = I_1' k_1 k_2^2 T_1^2 T_2^2 \exp(-\gamma l) \tag{3-2}$$

where, T_2 is the transmission coefficient at a glass–water interface. At normal incidence, T_1 and T_2 can be calculated from the Fresnel equation $T = 4n_1n_2/(n_1 + n_2)^2$, where n_1 and n_2 are the indices of refraction on each side of the interface. Assume the refractive index of the glass is 1.50 and that of the water is 1.33 [27]. If the attenuation of light in the air before the beam is incident on the cell is assumed to be 10^{-3}, then the average attenuation coefficient of light in the water can be obtained from Eqs. (3-1) and (3-2):

$$\gamma = \frac{1}{l} \ln \left(0.928 \frac{I_2'/I_1'}{I_2/I_1} \right) \tag{3-3}$$

3.3 Experimental results

Figure 19 shows the experimental results. The measurements were made using a laser with either a narrow-bandwidth (with injection seeding) or with wide-bandwidth (without injection seeding). For each length of the water cell, 10 groups of data were recorded; the results in Fig. 19 are the average values with error bars. Three special features can be seen. (i) For the wide-bandwidth laser the attenuation coefficient is constant, while for the narrow-bandwidth laser it increases with increasing pulse energy above some threshold. (ii) For the narrow-bandwidth laser, the slope of the attenuation coefficient vs. pulse energy decreases with the increasing

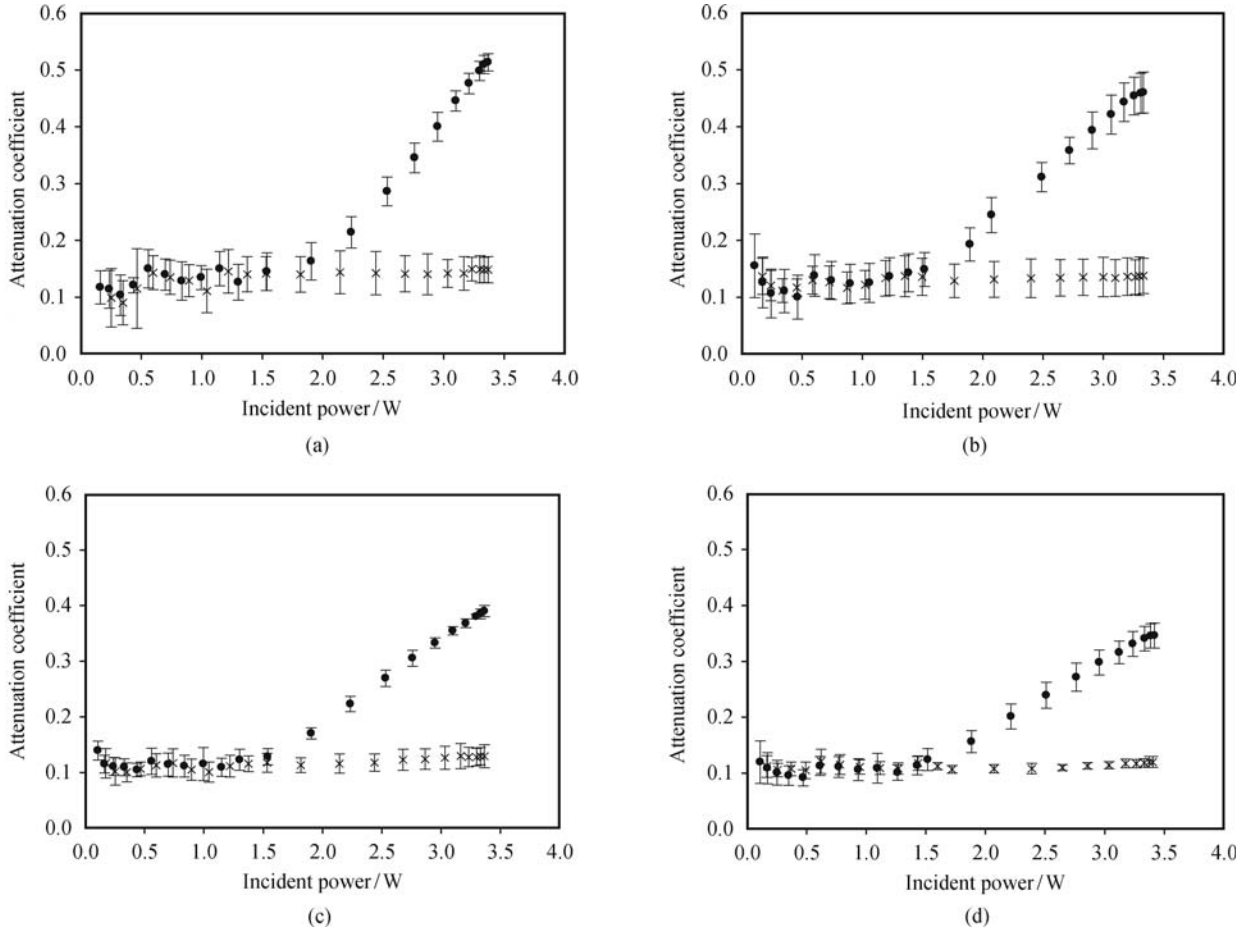

Fig. 19 Experimental measurements of attenuation coefficient of pulse laser beam in water. "•" represents the measured results with narrow-bandwidth laser beam. "∗" represents the measured results with wide-bandwidth laser beam. **(a)** $l = 0.8$ m; **(b)** $l = 1.2$ m; **(c)** $l = 1.6$ m; **(d)** $l = 2.0$ m.

length of the water sample. (iii) For every length of water cell the values of the attenuation coefficient of the narrow-bandwidth laser and the wide-bandwidth laser are the same when the pulse energy is small, but they diverge when the pulse energy is increased beyond a certain value. For a water cell length of 0.8 m this value is 175 mJ, for the other cell lengths it is about 150 mJ.

To demonstrate spontaneous and stimulated Brillouin scattering in the water, Fig. 20 (a) and (b) show the scattering spectra from the same position in the water when the pulse energy of a narrow-bandwidth (90 MHz) laser is lower or higher than the threshold value, respectively. For these measurements, the back-scattered light was collimated by a telescope system, and passed through a solid F–P etalon whose surfaces had 99.5% reflectivity at 532 nm. The scattered spectra were then recorded with an ICCD camera (Princeton Instruments PI-MAX2-1003). Figure 20 (a) and (b) clearly show that, when the pulse energy is lower than the threshold value, both the Stokes line and the anti-Stokes line appear in the spectrum. However, when the laser pulse energy is above the threshold value, only the Stokes line appears in the spectrum, and its intensity is much higher than that of Rayleigh scattering. This is the signature of SBS.

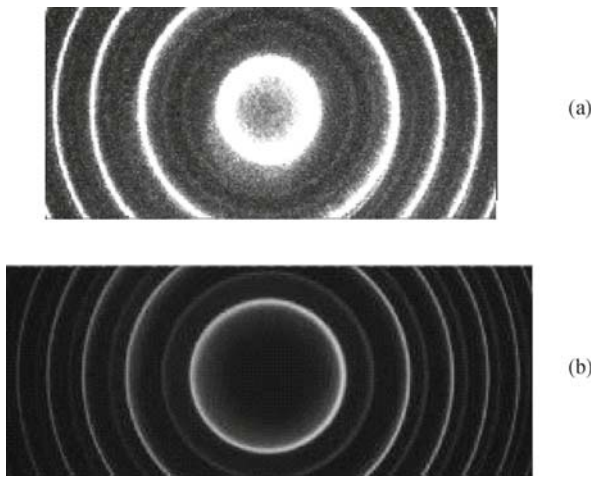

Fig. 20 Measured scattered spectra of narrow-bandwidth laser beam in water. The wavelength of the laser is 532 nm. The two spectra are measured at same position in water. **(a)** Spectrum of spontaneous Brillouin scattering when the pulse energy of the laser beam is lower than the threshold value; **(b)** Spectrum of stimulated Brillouin scattering when the pulse energy of the laser beam is higher than the threshold value.

3.4 Analysis and discussion

The above experimental results can be explained as foll-

ows. For the wide-bandwidth laser, attenuation is dominated by absorption and spontaneous scattering in the water. Consequently, the attenuation coefficient will be constant. However, for the narrow-bandwidth laser, SBS begins to dominate if the pulse energy is larger than the threshold value in water. The effect is to induce an extra attenuation of the forward propagating laser energy.

Stimulated Rayleigh-wing scattering [28] and stimulated thermal scattering [29] can be excluded from our experimental results due to their special properties. Also, according to Refs. [19, 30], the threshold value of stimulated Raman scattering is much higher than that of SBS. Consequently, the major component of the back scattering in our experiments could only be SBS. Calculations show that the coherence length of our laser was larger than the effective interaction length for SBS in the water. Thus, if a high pulse energy is used, the scattering can be considered narrow band SBS [31, 32]. On the other hand, since the pulse width of our laser is much greater than the lifetime of the stimulated phonon, stable theory for SBS is satisfied. Thus, the coupled wave equations are [19]

$$\frac{\partial I^p}{\partial z} = -gI^pI^s - \alpha I^p \tag{3-4}$$

$$\frac{\partial I^s}{\partial z} = -gI^pI^s + \alpha I^s \tag{3-5}$$

where, I^p is the intensity of the incident light, I^s is the intensity of SBS, α is the absorption coefficient of the water, and g is the gain of SBS. For simplicity, assume that only a small part of the energy becomes SBS, i.e., the energy converted into SBS is much less than the energy loss through absorption. From Eq. (3-4), we make the approximation

$$\frac{\partial I^p}{\partial z} = -\alpha I^p \tag{3-6}$$

By solving Eqs. (3-5) and (3-6), the intensity of SBS at a distance z in the medium is

$$I^s(z) = I^s(l)\exp\left[\frac{gI^p(0)(\mathrm{e}^{-\alpha z} - \mathrm{e}^{-\alpha l})}{\alpha} - \alpha(l-z)\right]$$
$$I < I_C^M \tag{3-7}$$

where, I_C^M is the coherence length of the laser, l is the effective interaction length of SBS, $I^s(l)$ is the intensity of spontaneous scattering at the end of the water cell, and $I^p(0)$ is the intensity of the laser beam at the beginning of the water cell. It can then be shown that the effective interaction length of SBS in the water is $l \approx 1$ m. Since $\alpha \leqslant 0.1$, $\alpha l \ll 1$, Eq. (3-7) can be rewritten as:

$$I^s(z) = I^s(l)\exp\left\{[gI^p(0) - \alpha](l-z)\right\} \tag{3-8}$$

Assuming that the attenuation in water is caused only by absorption and SBS in the water, the average attenuation coefficient is

$$\gamma = -\ln\left\{\exp(-\alpha l) - \frac{I^s(l)}{I^p(0)}\exp\left[gI^p(0) + \alpha\right] l\right\} \Big/ l \tag{3-9}$$

Figure 21 shows the attenuation coefficient simulated by Eq. (3-9) in a water cell of 1 meter length. In the figure, the horizontal axis $K = [gI^p(0)+\alpha]/l - 30$ is a linear function of the incident intensity. The simulated result is in good agreement quantitatively with the experimental results shown in Fig. 19. It should be noted that the value, 0.045–0.05 m^{-1}, for the previously recorded attenuation coefficient of light was measured in pure water. But since tap water was used in our experiments, our measurements of the constant attenuation coefficient are larger.

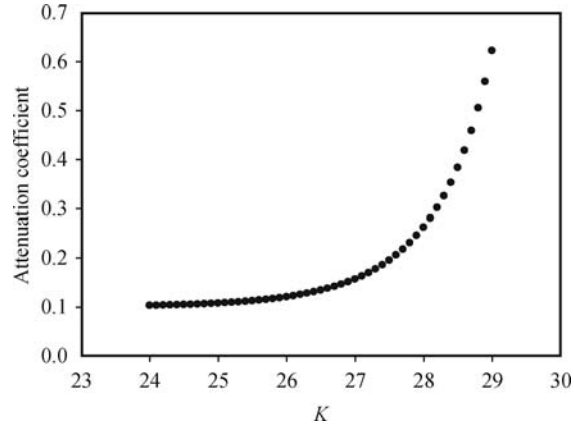

Fig. 21 Calculated attenuation coefficient of in the water cell of 1 meter. $K = [gI^p(0) + \alpha]/l - 30$.

Theoretical analysis shows that since the pulse width of our laser is 8 ns, the maximum length over which SBS can develop sufficiently in water is about 1 meter. We define this value as free gain length (FGL). In our experiments, four different cell lengths for the water samples were used. The 0.8 m long cell is less than the FGL in water, thus SBS will develop over the whole length of the sample. However, for the other three cells, the water samples are longer than the FGL. Thus, for those cells in the region beyond the FGL (1 m), the laser beam will propagate with spontaneous scattering (and smaller constant attenuation) rather than with SBS (and larger attenuation). The longer the water sample, the longer the length of the segment over which there is spontaneous scattering and hence reduced attenuation. Since the attenuation coefficient is an averaged value, the smaller constant attenuation will result in a decrease of the overall average attenuation coefficient. This explains the above mentioned special feature (ii) in our experiments; i.e., the slope of the attenuation coefficient vs. pulse energy decreases with increasing length of the sample cell.

If the length of the water sample is longer than the

FGL, SBS will develop adequately. On the other hand, for the 0.8 m cell length (which is less than the FGL), the development of SBS will be limited, and the threshold value is a little bit higher. This explains the special feature (iii) in our experiments.

3.5 Conclusion

If a narrow line width, high power laser is used for water applications, the attenuation coefficient of light in water is not constant. It will increase with increasing laser intensity if the intensity is larger than the threshold value for SBS.

4 Threshold value of stimulated Brillouin scattering [33, 34]

4.1 Background

Stimulated Brillouin scattering (SBS) has attracted general attention owing to its broad applications. Its characteristics and some important parameters had been investigated and reported [14, 19, 35–38], among which the threshold value is most important. Usually, the threshold value of SBS in terms of laser-intensity is determined by measuring the intensity of the back scattered SBS signal; when it reaches 2%, 3%, or 5% of that of the pumped laser beam, the latter can be considered as the threshold value [35]. Obviously, it is difficult to judge the first occurrence very accurately. Different researchers may choose different percentages. Therefore, different threshold values may be obtained when repeated measurements are made in the same material even in the same conditions.

Therefore, setting a standard and accurate method for determining the threshold value of SBS becomes important. Based on the work mentioned in Section 3, a new method for measuring the threshold value of SBS in terms of the laser-intensity is proposed. It is described as follows.

4.2 New method for measuring threshold value of SBS [33]

Water was chosen as the sample in our experiments. In our works, only the case of narrow band SBS was considered. It is known that if the line width of the laser used is narrower than the line width of Brillouin scattering, narrow band SBS [32, 40] will occur. Moreover, since stimulated Rayleigh-wing scattering [38] and stimulated thermal scattering [28] can be excluded due to their special properties, and, according to Refs. [29, 30], the threshold value of stimulated Raman scattering is much higher than that of SBS, the scattering happening in water could only be SBS if the pulse energy of the laser is controlled in a certain range. Thus, when a wide line width laser is used, the attenuation coefficient of water will be a constant. However, it will change when SBS occurs [22] with the use of a narrow line width laser. It means that, one can measure the attenuation coefficient of water, if the curve of the attenuation coefficient vs. pulse energy of the laser measured using narrow line width laser deviates from that measured with wide line width laser, the deviating point should be the threshold value of SBS.

The set-up geometry shown in Fig. 18 was used for measuring the threshold value of SBS. The output of the laser used was a pulsed TEM_{00} mode Gaussian beam with pulse width of 8 ns, divergence of 0.45 mrda, and the diameter at the output coupler is 8 mm. The two detectors used were two power meters (Coherent FIELDMATE and Newport 1835-C respectively). In the experiments, measurements were made under different pulse energies. In order to keep the output characteristics of the laser unchanged, the pulse energy of the laser was adjusted through changing the time delay between the oscillator and the amplifier, and the time delay was controlled by a DG 535 Digital Delay/Pulse Generator. The lengths of the water in the water cell were 0.4, 0.8, 1.2, 1.6 and 2.0 m, respectively. The water used was tap water sieved through a filter with 1 μm holes. Figure 11 shows the measured scattering spectra of spontaneous and stimulated Brillouin scattering induced by laser beam with a pulsed energy lower and higher than the threshold value of SBS in water respectively.

Figure 22 gives the average of 10 groups of data of the measured results of the attenuation coefficient in 1.6 m water cell by using wide and narrow line width lasers respectively, the error bars are also given. It can be found that the attenuation coefficient in the two cases deviate at a critical value of the pulse energy of the laser

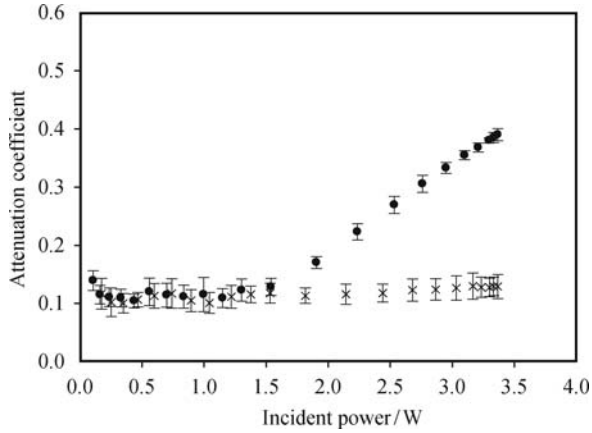

Fig. 22 Experimental measurements of attenuation coefficient of water in 1.6 m water cell. "•" represents the measured results with narrow-bandwidth laser beam. "∗" represents the measured results with wide-bandwidth laser beam.

which is considered as the threshold value of SBS in water. To determine the threshold value of SBS accurately, the measured results were fitted into two curves and are shown in Fig. 23 when the lengths of the water cell used were 1.2, 1.6, and 2.0 m, respectively.

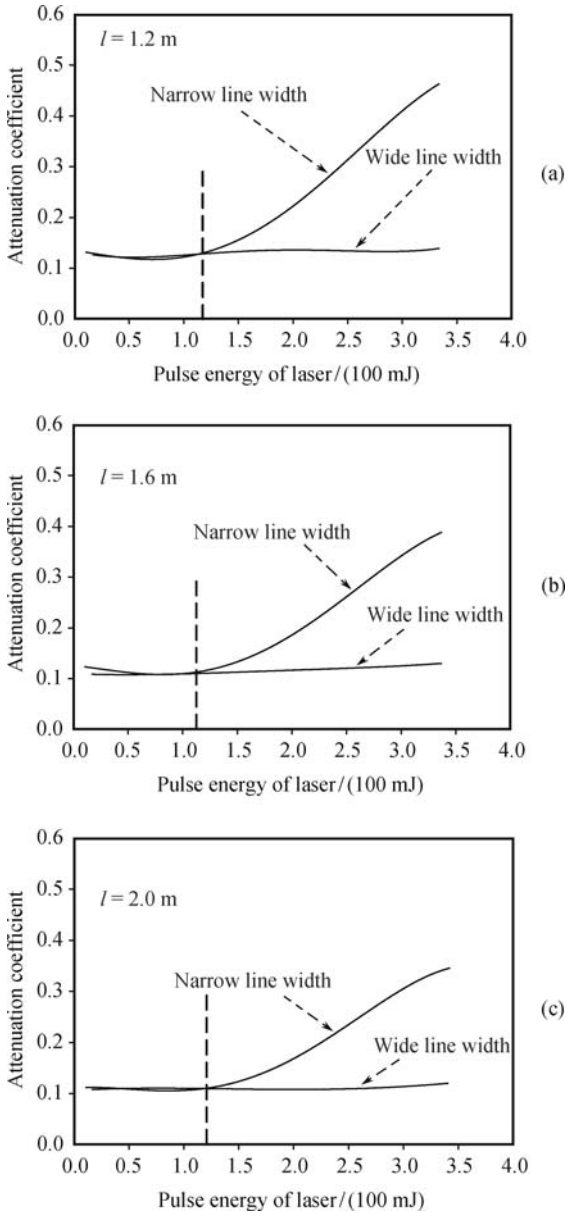

Fig. 23 Fitted curves of the measured attenuation coeffcient taken in water cells of 1.2, 1.6, and 2.0 m, respectively. The vertical dashed lines represent deviating points which correspond to che threshold value of SBS in water.

Now, the free gain length (*FGL*), the half-value of the product of the speed of light and the pump laser pulse width, is actually a range of length in which SBS will occur in the time period of one pulse width of the pump laser. It can be calculated by $FGL = \dfrac{V_{\mathrm{L}} \times \Delta t}{2}$, where V_{L} is the light speed in water and Δt is the pulse width of the laser. In our experiments, it is about 1 meter. Then, it can be seen clearly that, for the three water cells, the actual interaction lengths are all longer than the FGL, Thus, the SBS occurring in the cells must be steady state SBS, The threshold values of the pump laser peak intensity in these cells are 28.85, 28.60, and 29.59 MW/cm^2, corresponding to output pulse energy of 116, 115, and 119 mJ per pulse, respectively. Because their relative errors are all less than 2%, their average value 29.01 MW/cm^2 can be taken as the actual threshold that corresponds to 117 mJ per pulse.

Figure 24 gives the measured results taken in water cells with lengths of 0.4 m and 0.8 m, respectively. For these two cells their actual interaction lengths are all less than the FGL of the water, the SBS occurring in these cells is not steady state SBS, but it is also not true transient SBS. Both of the threshold values measured in the two cells (268 mJ and 160 mJ per pulse, respectively) are larger than 117 mJ, which is the average threshold value of steady state SBS in water. It shows that in the region slightly less than FGL of the water, the threshold value of SBS increases with the decrease of the length of the material. When the length of the water is even less, the true transient SBS is very difficult to achieve in a very short water cell because the threshold value becomes very high. On the other hand, the lasers with ps or fs pulse width are all wide line width, single mode SBS cannot be induced with them.

It should be pointed out that, though the threshold value of SBS is usually expressed by pump laser peak intensity, the pulse energy of the laser corresponding to the peak intensity is still given in the present work because the output pulse energy can be measured accurately in the experiments. In fact, the pump laser peak intensity is calculated based on the pulse energy measured using the parameters of the laser used. These values were pulse width of 8 ns, divergence of 0.45 mrad, and beam diameter of 8 mm at the output coupler for a TEM00 mode Gaussian beam. Using these parameters, one can estimate other values to express the threshold of SBS, such as the average energy density or the average power of the pulsed laser beam.

4.3 Theoretical discussion on threshold value of SBS [34]

Generally, the threshold value of SBS is considered as variable, even for the same material. Theoretically, the definition of the threshold value of SBS is based on back scattering (Stokes line). For steady state SBS, assuming that there is no depletion of the pumped laser beam and only the absorption by the scattering in the material is considered, the coupled wave equation of SBS can be expressed as:

$$\frac{\mathrm{d}I_{\mathrm{L}}}{\mathrm{d}z} = -\alpha I_{\mathrm{L}}, \quad \frac{\mathrm{d}I_{\mathrm{S}}}{\mathrm{d}z} = -g_{\mathrm{B}} I_{\mathrm{L}} I_{\mathrm{S}} + \alpha I_{\mathrm{S}} \tag{4-1}$$

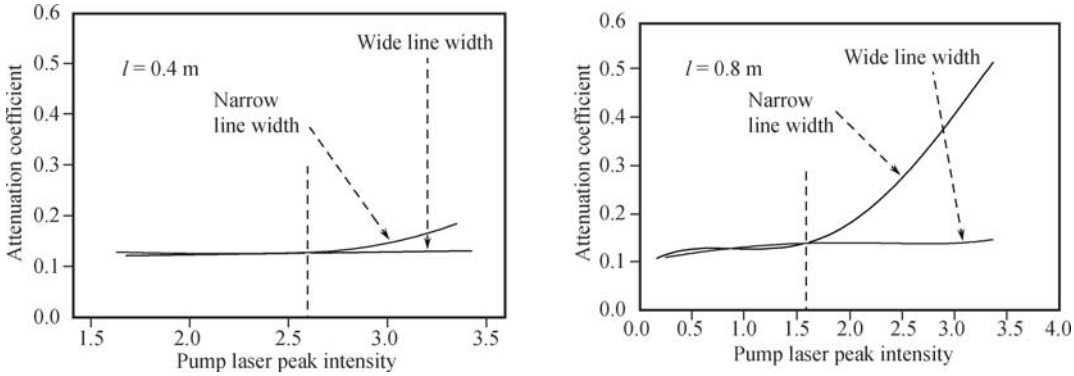

Fig. 24 Fitted curves of the measured attenuation coefficient taken in water cells of 0.4 m, and 0.8 m respectively. The vertical dashed lines represent deviation points which corresponding to the threshold value of SBS in water. The value per division of the horizontal axis is 24.87 MW/cm^2 which corresponds to an output pulse energy of 100 mJ.

where, $I_{\rm L}$ is the intensity of the pumped laser beam, $I_{\rm S}$ is the intensity of the back scattered light, α is the absorption coefficient of the material, $g_{\rm B}$ is the gain of the SBS in the material. Solving Eq. (4-1), we obtain

$$I_{\rm S}(z) = I_{\rm S}(L)\exp\left[g_{\rm B}I_{\rm L}(0)(\mathrm{e}^{-\alpha z} - \mathrm{e}^{-\alpha l})/\alpha - \alpha\,(l-z)\right] \tag{4-2}$$

Here, l is the length of the material. In the case of $\alpha l \ll 1$, we have

$$I_{\rm S}(z) = I_{\rm S}(l)\exp\{[g_{\rm B}I_{\rm L}(0) - \alpha](l-z)\} \tag{4-3}$$

Then, at $z = 0$, the intensity of the SBS is

$$I_{\rm S}(0) = I_{\rm S}(l)\exp\{[g_{\rm B}I_{\rm L}(0) - \alpha]l\} \tag{4-4}$$

Traditionally, the empirical relation $I_{\rm S}(l) \approx I_{\rm L}(0) \cdot \exp(-30)$ is used. Hence, the following condition would be satisfied when the intensity of the scattered light is of the same order of magnitude of the laser beam

$$I_{\rm Lth} \geqslant \frac{30 + \alpha l}{g_{\rm B} l} \tag{4-5}$$

This $I_{\rm Lth}$ is generally considered as the threshold value of the SBS in terms of the laser intensity, and it is related to the length l of the material. Here, $I_{\rm Lth}$ is directly related to the length l of the material. It means that different $I_{\rm Lth}$ would be obtained for the same material with different l, even for the same material under the same experimental conditions. This is obviously unreasonable. Therefore, it is very important to define a rigorous threshold value of SBS theoretically. In this paper, a new definition of threshold value of SBS in terms of laser intensity is put forward.

First, let us consider a concept – Real Gain Length (RGL). It can be defined as the length through which SBS occurs and is coherently amplified in the time period of a laser pulse. Though this analysis is based on steady state SBS pumped by single longitude mode laser, it also applies to transient SBS or quasi-steady state SBS, even in the case when SBS is pumped by multi-longitude mode laser after reasonable expansion. It is now discussed in detail as follows.

(1) For single longitude mode laser pumping

Let us consider the case in which the narrow line width pump laser has a pulse length L_p corresponding to the pulse width. When FWHM was chosen as the line width, the coherent length $L_{\rm c}$ of the laser can be considered as equal to the pulse length L_p, i.e., $L_c = L_p$. In this case, RGL will reach its maximum, that is $RGL_M = L_P/2 = L_{\rm c}/2$. For a CW laser, it can be considered as a pulsed laser with infinite pulse width. Actually, a pulsed laser can be taken as a CW laser when its pulse width is long enough. Because the line width of a single longitude mode laser cannot be considered as a delta function, therefore, $L_{\rm c} < L_p$. If RGL is considered as the maximum gain length for each monochromatic component, then we still have $RGL_M = L_{\rm c}/2$. Table 1 gives the coherent lengths and $RGLs_M$ of the lasers with different line widths in the air and in the water.

Table 1 Coherent lengths and RGL_M of lasers with different line widths.

Linewidth	Coherence length		RGL_M	
	In air	In water	In air	In water
500 MHz	0.6 m	0.45 m	0.3 m	0.225 m
100 MHz	3 m	2.25 m	1.5 m	1.125 m
90 MHz	3.33 m	2.498 m	1.667 m	1.249 m
5 MHz	60 m	45 m	30 m	22.5 m
200 kHz	1500 m	1125 m	750 m	562.5 m
10 kHz	30 km	22.5 km	15 km	11.3 km
1 Hz	3.0×10^8m	2.25×10^8m	1.5×10^8m	1.13×10^8m

(2) For multi-longitude mode laser pumping

In this case, the line width is of the total modes of the laser instead of each mode. For a pulsed laser, $L_{\rm c} \neq L_p$. However, the physical significance of the coherent length does not change. Therefore, we still have $RGL_M = L_{\rm c}/2$. For a CW laser, $L_{\rm c}$ and L_p are not comparable, but $RGL_M = L_{\rm c}/2$ is still correct.

(3) Effect of material length $L_{\rm m}$

The above discussions are all based on the assumption that the length of the material is infinite. How-

ever, it also works well for finite length materials when $L_c < 2L_m$, because in this case RGL can still reach the maximum. However, if $L_c > 2L_m$, then, $RGL_M = L_c/2$, and cannot reach the maximum. It actually means that when the interaction length between the SBS and the pump laser beam equals to the RGL, the SBS has already developed sufficiently. The part of the laser beam beyond the material length L_m will not induce sound wave in the material. Thus, the effect of material length L_m is very important for the SBS in long materials excited by a very narrow line width laser, for example the SBS excited by narrow line width laser in fiber. According to Table 1, for a laser with line width of 10 kHz, the RGL in air is 15 km, the RGL corresponding to that in silicon is about 10 km. Therefore, the length of the fiber should be long enough in order to maintain stability and reliability of SBS, that is the reason why Tomoya *et al.* [41] chose the fibers longer than 20 km for measuring the threshold value of SBS in their experiments.

According to the above discussions, the coherent length L_c and the material length L_m are the key factors related directly to Real Gain length RGL, and RGL can be expressed as:

$$RGL = \min\left(\frac{L_c}{2}, L_m\right) \tag{4-6}$$

i.e., RGL should be chosen as the minimum value among the material length L_m and one half of the coherent length L_c of the laser, where, the sign $\min(\cdot)$ represents choosing the minimum value of the parameters inside it.

Then, the threshold value of SBS would be analyzed based on the concept of RGL. The terms "steady state" or "transient" SBS refer to the changing character of the SBS with time. Let τ_B be the lifetime of phonon, and τ_c expressed as $\tau_c = RGL/\upsilon_p$ be the interaction period between the laser and the material, where, υ_p is the light speed in material. The value of τ_c relative to τ_B determines whether the SBS that will occur is steady state or transient. It should be pointed out that, there is no practically clear cut critical point between "steady state" and "transient" cases. It can only be determined empirically.

(1) $\tau_c \gg \tau_B$

When $\tau_c \to \infty$, ideal steady state SBS would occur. It can be taken as steady state SBS when $\tau_c > 100\tau_B$. From Eq. (3-4) and considering the physical mechanism, as long as the Brillouin gain is larger than the absorption of the material, i.e., $g_B > \alpha$, SBS can occur and be amplified. Therefore, the threshold value of steady state SBS will be

$$I_{Lth} = \frac{\alpha}{g_B} \tag{4-7}$$

It can be seen obviously that $I_{Lth}$is independent of the length of the material, and only related to the characters of the material such as Brillouin gain and absorption coefficient. It means that the threshold value of steady state SBS will be a constant for a certain material. In the following cases, SBS would be steady state: the SBS excited by single longitude mode CW laser in a very long fiber; SBS excited by single longitude mode laser with long pulse in long material, which in fact corresponds to the case of SBS elicited in the Herriot set-up [42] or in an F–P [43] using single longitude mode CW laser or single longitude mode laser with long pulse width, in which the light repeats in the etalon just like it passes a long material.

(2) $\tau_c \ll \tau_B$

When $\tau_c \to 0$, ideal transient SBS could occur. It can be taken as transient SBS when $\tau_c < 0.01\tau_B$. Kroll [38] and Hon [39] investigated the threshold of SBS when interaction period is less than or equal to the lifetime of the phonon. Their investigations were still based on the empirical relation $I_S(l) \approx I_L(0)\exp(-30)$. However, it can be discussed without this empirical relation and based only on the physical mechanism. By solving three wave coupled wave equation (i.e., including sound wave), and neglecting the depletion of the pumped beam, the intensity of SBS is [19]

$$I_S(z,t) = I_S(l,t)\exp\left\{2\left[(g_B I_L(0) - \alpha) \cdot (l-z)\, t/\tau_B\right]^{1/2} - t/\tau_B\right\} \tag{4-8}$$

The threshold value of SBS can now be defined. According to the physical mechanism of SBS, when $2\left[(g_B I_L(0) - \alpha)(L-z)\, t/\tau_B\right]^{1/2} \geqslant t/\tau_B$, the scattered light can be amplified during its propagation. Therefore, when SBS occurs, the following equation will be satisfied at position z:

$$2\left[\frac{g_B}{\tau_B}(l-z)\int_0^{t_L} I_L(t')\,\mathrm{d}t' - \frac{\alpha}{\tau_B}(l-z)\, t_p\right]^{1/2} \geqslant \frac{t_p}{\tau_B} \tag{4-9}$$

where t_p is the pulse width of the laser. Assuming that the pulse is rectangular, when $t_p < \tau_B$, we have

$$I_{Lth} \geqslant \frac{t_p}{4g_B\tau_B(l-z)} + \frac{\alpha}{g_B} \tag{4-10}$$

It can be seen that, different from the case of steady state SBS, this threshold value is a variant, and related not only to the characteristics of the material but also to the pulse width and the propagation length of the back scattered light.

However, Eq. (4-10) is not the threshold value of the ideal transient SBS. Ideal transient SBS only occurs when the pulse width of a laser is much less than the lifetime of a phonon. Because the back scattered light induced by the front of the laser pulse will be amplified by the light of the tail of the laser pulse, the scattered

light will propagate a length of $\frac{t_p v_p}{2}$ in the time period of the effective interaction. Substituting $(l-z)$ by $\frac{t_p v_p}{2}$ in Eq. (3-10), and neglecting dispersion effect, we have

$$I_{\mathrm{Lth}} \geqslant \frac{2}{4 g_{\mathrm{B}} \tau_{\mathrm{B}} v_p} + \frac{\alpha}{g_{\mathrm{B}}} \tag{4-11}$$

Practically, there is another case, i.e., the pulse width of the laser may not change, but the length of the material becomes shorter, which makes the interaction period of the scattered lights become shorter. It is actually the case of $RGL = L_{\mathrm{c}}/2$. Though the whole laser pulse can pass through the material, the scattered light induced by the front of the laser pulse may not interact with the light of the rear part of the pulse, and the effective interaction length will be short, i.e., RGL will be shorter. In this case, RGL is determined by the length of the material. Therefore, the effective interaction period is the length of interaction determined by the length of the material, which leads to $t_e = \frac{2L_{\mathrm{m}}}{v_p}$. As long as L_{m} is short enough, what occurs will be transient SBS. Substituting $t_e = \frac{2L_{\mathrm{m}}}{v_p}$ into Eq. (4-10), the threshold value obtained is still Eq. (4-11).

According to the above analysis, the threshold value of ideal transient SBS is still a constant, and is related only to the characteristics of the material. Through Eq. (4-11), the threshold value of transient SBS is estimated to be about 5 orders of magnitude larger than that of steady state SBS.

(3) Other cases

Practically, what occurred mostly is neither ideal steady state SBS nor ideal transient SBS, in which the distribution of the phonons is in relaxation state from thermal equilibrium to non-equilibrium stationary state. In this case, the threshold value is not only related to characteristics of the laser and the material but also to RGL rather than related directly to the coherent length L_{c} of the laser or the material length L_{m}. Whether it varies with the change of the lengths of the material is determined by the relationship between RGL and the lengths of the material. If RGL is related only to the coherent length L_{c} of the laser, the threshold will be independent of the lengths of the material. If the length L_{m} of the material is less than the coherent length L_{c} of the laser, RGL will be dependent on the lengths of the material. In this case, the threshold value of SBS in terms of laser intensity will be related to the material lengths, and it should be measured individually for a specific set-up geometry.

From the above discussions, the threshold value of steady state SBS (ideal steady state and its approximations) is most commonly significant, and it is the minimum in all pumping conditions. The ideal transient SBS is difficult to achieve because of high threshold. For other practical cases, the threshold should be measured actually. Discussing whether what occurred was steady state or transient SBS without considering the practical case is unreasonable.

4.4 Conclusion

Experimentally, the threshold value of SBS in terms of laser intensity can be measured accurately by measuring the attenuation coefficient of the laser beam with narrow line width and wide line width respectively. Theoretically, the threshold value of SBS is deducted rigorously based on a new definition of Real Gain length (RGL). This deduction is achieved without using any empirical formula. The threshold values of steady state and transient SBS are both constant and are independent of material length.

5 Stimulated Raman scattering enhanced by stimulated Brillouin scattering [44, 45]

5.1 Background

Stimulated scattering in liquid is an important research topic in Physics and Chemistry [19, 28, 29, 46, 47]. SBS and stimulated Raman scattering (SRS) are two important nonlinear processes. Generally, these two kinds of scattering are in competition [48–53]. If the pumped laser beam is multi-longitude mode with wide line width, the forward SRS (FSRS) will be dominant [54], and both SBS and backward SRS (BSRS) will be greatly suppressed. When the pumped laser beam is single longitude mode, in a gas under several tens of atmospheric pressure, both SBS and SRS can occur, and the SBS will be dominant, since most energy of the pumped laser beam is converted to SBS. For FSRS and BSRS, the difference of their gains is negligible because of the use of narrow line width pumping laser. However, since the direction of the BSRS is the same as that of the SBS, some energy of the laser may still be utilized, while the FSRS can absorb the energy from the residual forward laser energy only. Thus, it can hardly be amplified effectively. Certainly, one can decrease the SBS gain in gas by changing the density of the gas. Also, the SBS gain in gas can be controlled by changing its constitution, for example, Jones *et al.* [48] added CH_4 in gas He in their experiment. Different from the case in gas, the parameters in liquids are almost constants. The density of liquid can hardly be changed, even under extremely high pressure. Therefore, the gain of steady state SBS in liquids is generally stable. The competition between SRS and SBS depends on whether the pulse width of the laser used is longer than the lifetime of the phonon. The typical lifetime of

the acoustic phonon in liquids is in the magnitude of ns, while the lifetime of the optical phonon is about the magnitude of ps. When a Q-switched pulsed laser with the pulse width of ns interacts with the liquid, the SRS with fast relaxation will reach stability first and absorb some energy from the laser beam stably. On the other hand, though the SBS with higher gain builds up slowly, it will finally be dominating, and will draw out most of the energy from the pumped laser beam. Therefore, the SRS will be suppressed though it occurred earlier. However, some works show that pumping effect exists between SBS and SRS in liquid. Zhang *et al.* realized pumping effect of SBS on SRS in alcohol by focusing certain illumination with a single mode laser [55]. Different from the work by Jones, the medium they used was alcohol droplet; the particular shape of the droplet increased the interaction length between SBS and SRS. Recently, the present authors found that without using the particular shape of a liquid droplet, the energy amplification effect of SBS on BSRS can be obtained in the water in an optical cell the same as that used by Jones *et al.* with single mode laser. It is demonstrated that, besides the competition, there exists an enhancing effect of SBS on the BSRS. The experimental results together with the analysis are reported as follows.

5.2 Experiments

The experimental layout is shown in Fig. 25. An injection seeded pulsed Nd: YAG laser (Continuum Powerlite Precision Plus) was used. A narrow line width (90 MHz) and a wide line width (30 GHz) can be achieved respectively by switching the seeder on and off, the pulse repetition rate is 10 Hz, the pulse width is 8 ns, the maximal pulse energy is 1.5 J at 532 nm. The output energy of the laser was controlled through variation of the time delay between the amplifier and the oscillator to keep the stability of the laser. The power meters used were Coherent FIELDMATE, MOLECTRON PM500A and Newport 1835-C respectively. The length of the water cell is 2 m.

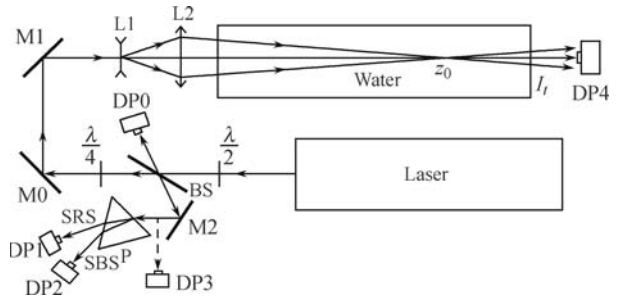

Fig. 25 Experimental layout. BS, $\lambda/2$, $\lambda/4$: polarized coupler, half wave and quarter wave plate at 532 nm respectively; M0–M2: mirrors. L1, L2: lenses; P: splitting prism; DP0–DP4: detectors.

The vertical polarized laser beam of 532nm changed into horizontal polarized after passing through $\lambda/2$ plate, so that most of the laser energy passes through BS, and only a small fraction was reflected. The reflected intensity I_1 was detected by DP0. The transmission intensity I_P can be monitored in real time by the transmission/reflection ratio of BS which is already known. The transmission beam turned into circularly polarized after passing through a $\lambda/4$ plate, then was reflected by M0 and M1 and focused at a certain point in the water cell. Under narrow band mode, SBS will appear at that point. Since SBS propagates only backward, it becomes vertically polarized after passing through the $\lambda/4$ plate. Most of the energy of the SBS is reflected by M2, and then it passes through a prism P to split into a first order SBS and a BSRS which are detected respectively by DP2 and DP1. The residual intensity of the laser will be transmitted through the other end of the water cell and detected by DP4.

In order to ensure comparability among the experimental data, the location of the water cell was shifted to adjust the position of the focal point of the laser in the water to ensure that the SBS obtained from different focal lengths have the same converging angle. Besides, the normal direction of the front and the rear surfaces of the water tank was slightly deviated from the direction of the laser beam with an angle of 5° so that the reflection beam of the two surfaces would not affect the received signal.

5.3 Experimental results and discussion

Figure 26 shows the measured spectrum. Figure 26 (a) shows the mean results of 7 groups of the measured data which were obtained using a narrow band laser beam with 0.15 J/pulse and focused at 1.5 m in the water cell. The backward conjugate scattered signals were received by a spectrometer at the location of DP3 shown in Fig. 25. The spectrum was normalized by the maximum value at 532 nm. Three peaks are shown: a peak at 532 nm consisting of Rayleigh scattering and Brillouin scattering, and two much lower peaks at 462 nm and 650 nm corresponding respectively to the blue shift and the red shift of the backward Raman scattering. Since the signals of Rayleigh scattering and Brillouin scattering cannot be differentiated by a simple single channel spectrometer, an FP etalon was used to analyze the detailed constitution of the peak at 532 nm. The result is shown in Fig. 26(b). The free spectral range of the etalon used is 22.4 GHz, and the recording instrument is an ICCD camera (PI-MAX2 1003, Princeton Instrument). The spectrum obtained is a typical SBS spectrum. The main component of the 532 nm peak is a very strong signal of SBS with a little frequency shift, while the signal of the Rayleigh scattering without any frequency shift is very weak and negligible. It demonstrated that

the SBS here dominates absolutely, while the intensity of the BSRS is two orders lower, though not inhibited totally.

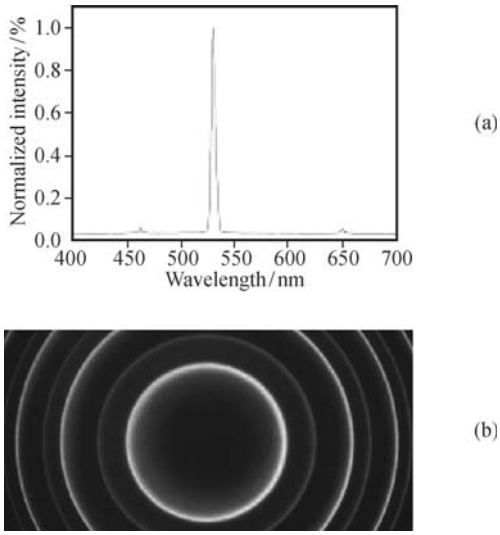

Fig. 26 Measured spectra of back scattered SBS. The laser with 0.15 J/pulse was focused at 1.5 m in the water cell. **(a)** Normalized spectrum using spectrometer; **(b)** Fine spectrum at 532 nm using F–P etalon.

Figure 27 shows the changes of the energies of SBS and BSRS with the change of the energy of the incident laser when the focal length was fixed at 1.5 m in the water. The left ordinate shows the energy of the SBS, the right ordinate shows the energy of the BSRS, while the abscissa shows the energy of the incident laser. It can be seen that the SBS energy increases with the increase of the laser energy, but the slope becomes lower gradually when laser energy is higher than 0.5 J and reaches its maximum at a laser energy of about 0.8 J, beyond which it begins to drop. However, the BSRS energy shows no increase at all until the laser energy becomes higher than 0.5 J, after which it increases rapidly and exponentially.

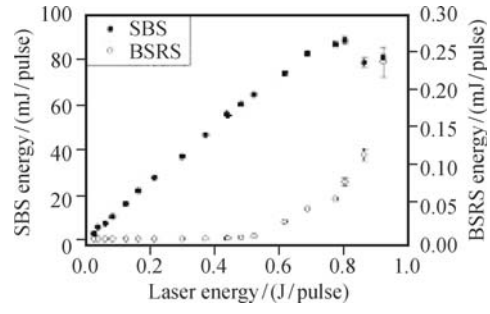

Fig. 27 Changes of SBS and BSRS energies with the change of laser energy when laser is focused at 1.5 m in water.

The medium used here is water which has higher steady Brillouin gain than gas, therefore the SBS process is always dominant, and the increase of BSRS shows only very slight influence on the increase of SBS. This is different from the case in gas where the two are always competing with each other.

The above variables were also observed when the laser was focused at a length of 0.5 m in the water tank. The results are shown in Fig. 28. After comparison between the data in Figs. 27 and 28, the following points could be noticed: when the focal length is 0.5 m, the length of the effective gain of the backward scattering is less than the coherent length of the laser, thus the transient effect should be taken into consideration. For SRS, the lifetime of the phonon of the optical branch is in the order of ps, the corresponding maximum gain length is in the order of cm, thus it is still under steady state; while for SBS, since the lifetime of acoustic phonon is in the order of ns, the corresponding maximum gain length is in the order of cm. It is much closer to the transient state as compared with the case of 1.5 m focal length. Considering that both SBS and BSRS are excited by the incident laser, it is reasonable to predict that under 0.5 m focal length the BSRS energy should stay unchanged, and the SBS energy should be decreased as compared with the case of 1.5 m focal length. However, as is shown in Fig. 28, this is not true! The BSRS signal under focal length of 0.5 m is much weaker than that under focal length of 1.5 m, while the SBS signal under focal length of 0.5 m is even stronger than that under focal length of 1.5 m. This implies that the BSRS and SBS produced by a single mode laser focused in water are not likely to be excited and maintained only by the laser pulse simultaneously.

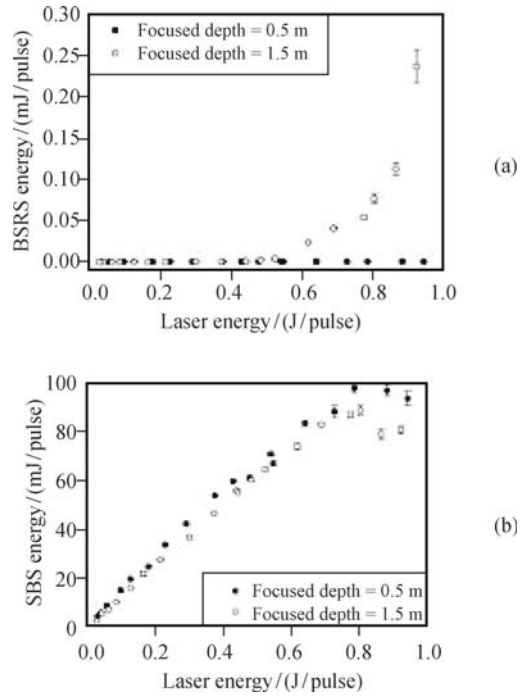

Fig. 28 Change of BSRS energy and SBS energy vs. change of incident laser energy when the laser is focused at 0.5 m and 1.5 m lengths, respectively, in the water tank. **(a)** Energy relationship: Incident laser vs. BSRS; **(b)** Energy relationship: Incident laser vs. SBS.

Different from the competition in a gas medium, the

relationship between SBS and BSRS in water is more complicated. Since the steady gain of SBS in liquid medium is one order higher than that of the BSRS [56], the SBS has definite superiority and draws most of the energy from the incident laser after initial competition; and the peak power of the SBS can possibly surpass the incident laser owing to the compression effect of the pulse width; when the intensity of the SBS reaches a certain value, it may have a strong enhancing effect on the weak BSRS signal transmitted synchronously. This interaction consumes a certain amount of energy from the SBS but greatly enhances the BSRS signal. This also explains why the BSRS through different lengths of water has different thresholds because all effective lengths are needed for both the accumulation of the SBS itself and the enhancement of the simultaneous BSRS.

The above points were verified by an experiment in which the energies of SBS and BSRS were measured under different focal lengths in water with the incident laser energy fixed at 0.62 J. The results are shown in Fig. 29. It can be seen that the SBS energy is about two orders higher than the energy of BSRS. If the two were considered to be competing with each other, both of them would acquire longer effective gain length and increased intensity with the increase of the focal length in the water. However, what we see from Fig. 29 is that the steady state single pulse energy of the SBS changes only a little when focal length is in the range of 0.2–0.8 m, and drops beyond 0.9 m. On the contrary, the single pulse energy of BSRS is very weak when the focal length is 0.2–0.8 m, but increased obviously beyond 0.8 m. Considering that this is similar to the commonly known phenomenon of the change of the forward SRS signal intensity with change of the interaction length [21], we can see that for the backward transmitted SBS and BSRS, the latter is just forward with respect to the former.

In order to show more visually the relationship between the SBS energy and the focus depth in water and the laser energy, Fig. 30 gives a 3-D plot of the experimental data. It can be seen that the relationship is shown as a 3-D curved surface. When the input laser energy is constant, the energy of SBS decreases with the increase of focus depth of the laser beam in water, and it is more obvious when the laser energy is high. It is similar to the result shown in Fig. 29. Besides, when the focus depth is larger than 1.1m, the energy of SBS changes non-monotonically with the increase of input laser energy, and reaches maximum. If the laser energy is lower than the maximum, the energy of SBS increases when the laser energy becomes higher, but, it will decrease with the increase of laser energy beyond the maximum. The reason may be that, in the case of shorter focus depth, (the back gain length of SBS is shorter), SBS is not built up sufficiently, although it is dominant. Therefore, SBS will be stronger gradually by drawing out the laser energy. However, if the focus depth is over 1.1m, SBS will be built up sufficiently. Therefore, SBS will only convert its energy to SRS propagating in the same direction, but also may excite some other nonlinear effect (for example, second order SBS) due to its very high peak power. When the dual energy consumption exceeds the energy which is drawn out from the laser, it will finally result in the reduction of SBS energy. Besides, for an identical laser energy, this process will have a stronger effect on SBS if the interaction length is large enough which is

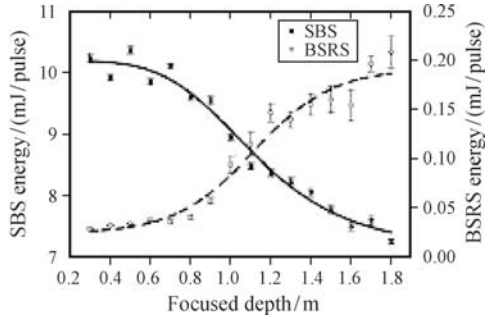

Fig. 29 The relationship between pulse energy of SBS and BSRS and focus depth in water. The pulse energy of incident beam is 0.62 J.

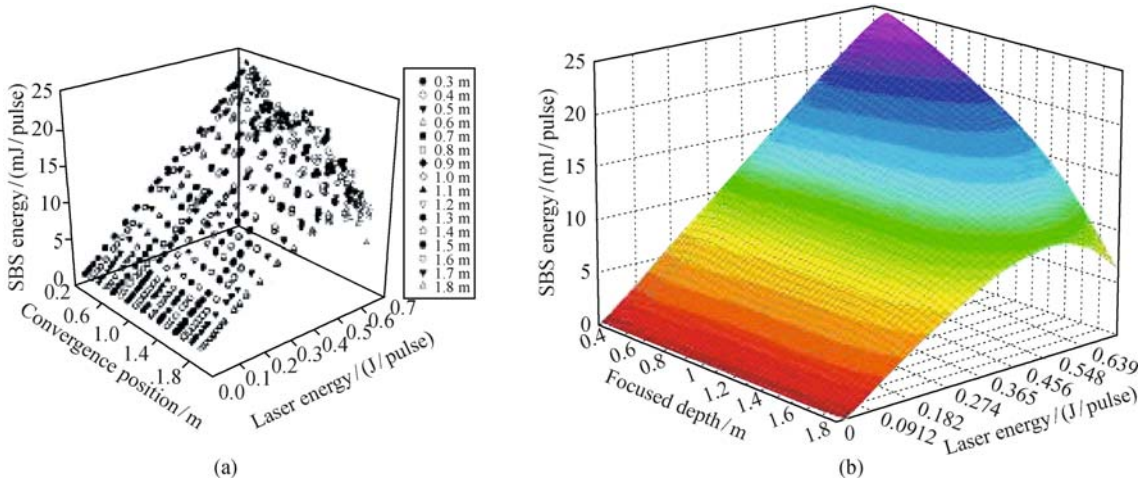

Fig. 30 3-D plot of SBS energy vs. focus depth of the laser beam and the laser energy. **(a)** Experimental data; **(b)** 3-D mesh plot.

induced by increasing the focus depth of the laser beam.

In order to understand the physical mechanism more clearly, the wave vector scheme during the process of the amplification is shown in Fig. 31. For SBS, its wave vector $\boldsymbol{K}_{\rm SBS}$ equals to the wave vector $\boldsymbol{K}_p$ of the laser minus the wave vector $\boldsymbol{K}_{\rm aB}$ of acoustic phonon. Similarly, for SRS, the wave vector $\boldsymbol{K}_{\rm FSRS}$ of amplified SRS equals to $\boldsymbol{K}_{\rm SBS}$ minus the wave vector $\boldsymbol{K}_{\rm aR1}$ of optic phonon.

Fig. 31 The wave vector scheme of the experiment, $\boldsymbol{K}_p$, $\boldsymbol{K}_{\rm SBS}$, $\boldsymbol{K}_{\rm aB}$, $\boldsymbol{K}_{\rm FSRS}$, and $\boldsymbol{K}_{\rm aR1}$ represent the wave vectors of laser, SBS, acoustic phonon, FSRS, and optical phonon, respectively.

The relationship between SBS and BSRS can also be seen from the time profile as shown in Fig. 32. Because of the optical layout in the experiment, the BSRS signal went 0.45 m longer more than the SBS along the path, which corresponds to a time delay of 1.5 ns, and the minimal value of SBS always accompanies the maximum value of BSRS. (The heights of the two curves in Fig. 32 are only for reference, they do not represent the actual intensities.) This means that there exists a strong time correlation between the intensities of the SBS and the BSRS, and this in turn shows the existence of an obvious energy transfer between the SBS and the BSRS. This phenomenon has also been found by Zhang and Chang in their studies of stimulated scatterings in liquid droplets [55]. They considered it to be the direct evidence of the pumping effect of the SBS on the SRS. However, this phenomenon was not found in the experiment using an optical cell. The medium they used was spherical shaped alcohol droplet. The special shape of the medium made the strongest intensity of the SBS signal along the 90° direction, and both the SBS and the BSRS were moving circularly surrounding the surface of the sphere to ensure an adequate length of interaction. Besides, the illumination they used was focused center illumination which avoided having the incident laser coupling into the surface layer of the alcohol droplet to form circular motion. If focused edge illumination were used in which the laser was coupled into the boundary of the droplet, it is still not considered that the SRS is mainly pumped by the SBS, but both of them come from the laser and are competing all the way.

In Jones's analysis [48], with the intensity and the length of the interaction, more and more laser energy would be converted to BSRS and BSRS would have more and more interaction period, so that the intensity of SBS would decrease greatly. However, from the experimental results shown in Figs. 27–29, even though the laser beam was focused at 1.5 m, SBS had been built up and amplified sufficiently. Therefore, Jones' theory cannot be used to analyze the experimental results mentioned above.

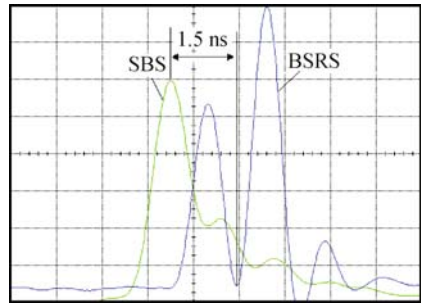

Fig. 32 Time profile of backward conjugated SBS and BSRS signals. Incident laser energy = 0.71 J, focal length = 1.5 m, abscissa 1.0 ns/div.

Our work demonstrated for the first time that SBS has a strong enhancing effect on BSRS in a water medium in a simple focused optic cell. This means that the pumping effect of SBS on BSRS is a commonly existing rule regardless of the experiment conditions.

As was known from the above, in the water medium of an optical cell, the strong SBS interacts with the backward SRS and transfers energy to the latter. There may be two possible physical mechanisms about the energy transfer in the interaction:

The first is the BSRS energy amplification by the SBS. As was known from the early works [50], SRS appears prior to SBS. SRS always exists even when the SBS appears. Then, the SBS draws most of the energy from the laser after it approaches steady state and inhibits the SRS to a very low level. When adequate energy is accumulated with the backward SBS, it may amplify the inhibited BSRS signal. Hence, the SBS is pumping the BSRS while it is pumped by the laser. Since the frequency difference between SBS and the laser is only 7.5 GHz, the linewidth of the SBS is about the order of hundreds of MHz, and the linewidth of the narrow band laser is 90 MHz, while the linewidth of the SRS is about 100 GHz, the spectra of the SRS excited by both the laser and the SBS are mostly overlapped, except that their centre frequencies are separated by 7.5 GHz. Therefore, most of the BSRS excited by the laser can be amplified by SBS. Under this picture, the longer the backward gain length is, the stronger the BSRS signal is.

The second possible mechanism is that an extremely strong SBS can excite its own forward SRS. When the energy of the incident laser is very high and the gain length is adequately long, SBS may have a very high peak power due to the pulse compression, once it surpasses the threshold of the second order SBS or SRS, SBS can possibly act as the source to excite a second order SBS or SRS. Actually, as shown in Fig. 33, we did observe a second order SBS in the forward direction of the incident laser, i.e., the backward direction of the first order SBS. Figure 33 shows the spectra of all the forward

transmitted signals through a 532 nm etalon. The spectrum of each order consists of three spectral lines. The outer line corresponds to the elastic scattering with the same frequency as the incident laser, the middle line b corresponds to the backward Rayleigh scattering excited by the first order SBS, while the inner line c corresponds to the second order SBS. Since the line width of the first order SBS is about five times that of the laser, the gain of the second order excited is no longer superior to SRS; it is possible that the first order SBS can excite a new SRS when its intensity is high enough.

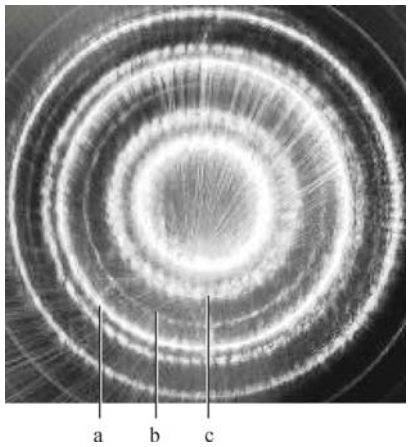

Fig. 33 FP spectra of laser transmitted through the back end surface of the water tank. Energy of the incident laser = 0.11 J, focal length = 1.5 m. **a:** Elastic scattering line, the same frequency as the incident laser; **b:** Rayleigh scattering excited by 1^{st} order SBS; **c:** 2^{nd} order SBS.

The forward SRS excited by the SBS itself is in the same direction as the BSRS; their spectral characteristics are difficult to distinguish, so it is hard determine which one is functioning. Maybe both of them occurred in the experiment, but one of them dominated the other under certain conditions. When the focal length is shorter, the self accumulation of the SBS is inadequate; its interaction length may be limited, even though SBS is excited. The first mechanism may be dominating under this condition, SRS here is excited mainly by the laser and only slightly amplified by SBS, and the total energy may still be very low. When the focal length is longer, the accumulation of SBS is adequate for exciting a second order SBS and FSRS. Therefore, both the two mechanisms are functioning, and even the second one may be dominant.

5.4 Conclusion

The relationship between SBS and BSRS excited by a laser in water was restudied. Experimental results showed that besides the conventional competition relation, a strong SBS has obvious pumping effect on BSRS transmitted synchronously. Analysis showed that there may be two possible mechanisms. Referring to the studies in spherical alcohol droplet reported by other authors, it is believed that this pumping effect exists generally in liquid media, regardless of the particular boundary shape.

Acknowledgements The authors would like to thank the National Advanced Technology Development program (Grant Nos. 2002AA633110 and 2009AA09Z101) and the National Natural Science Foundation of China (Grant Nos. 60778049, 10574016, 10274006, and 10904003) for financial support.

References

1. J. L. Guagliardo and H. L. Dufilho, Rev. Sci. Instrum., 1980, 51: 79
2. D. J. Collins, J. A. Bell, R. Zaoni, I. S. McDermid, J. B. Breckinridge, and C. A. Sepulveda, Proc. SPIE., in: Ocean Optics, edited by M. A. Blizard, 1984, 489: 247
3. J. G. Hirschberg, J. D. Byrne, A. W. Wouters, and G. C. Boynton, Appl. Opt., 1984, 23: 2624
4. G. D. Hickman, J. M. Harding, M. C. Garnes, Al. Pressman, G. W. Kattwar, and E. S. Fry, Remote Sens. Eviron., 1991, 36: 165
5. D. A. Leonard, and H. E. Sweeney, Proc. SPIE., in: Ocean Optics IX, edited by M. A. Blizard, 1988, 925: 407
6. E. S. Fry, Y. Emery, X. H. Quan, and J. Katz, Appl. Opt., 1997, 36: 6887
7. A. Popescu, K. Schorstein, and T. Walther, Appl. Phys. B, 2004, 79: 955
8. K. Schorstein, A. Popescu, M. Göbel, and T. Walther, Sensors, 2008, 8: 5820
9. J. W. Shi, M. Ouynag, W. P. Gong, S. J. Li, and D. H. Liu, Appl. Phy. B, 2008, 90: 569
10. W. P. Gong, J. W Shi, G. X. Li, D. H. Liu, J. W. Katz, and E. S. Fry, Appl. Phys. B, 2006, 83: 319
11. W. P. Gong, R. Dai, Z. H. Sun, J. W. Shi, and D. H. Liu, Appl. Phys. B, 2004, 79: 635
12. J. F. Xu, R. Dai, W. P. Gong, X. B. Ren, and D. H. Liu, Appl. Phys. B, 2004, 79: 131
13. R. Dai, W. P. Gong, J. F. Xu, X. B. Ren, and D. H. Liu, Appl. Phys. B, 2004, 79: 245
14. J. F. Xu, X. B. Ren, W. P. Gong, R. Dai, and D. H. Liu, Appl. Opt., 2003, 42: 6704
15. D. H. Liu, J. F. Xu, R. S. Li, R. Dai, and W. P. Gong, Opt. Commun., 2002, 203: 335
16. M. Ouyang, J. W. Shi, L. Zhao, X. Chen, H. Jing, and D. H. Liu, Appl. Phy. B, 2008, 91: 381
17. J. W. Shi, G. Li, W. Gong, J. Bai, Y. Huang, Y. Liu, S. Li, and D. H. Liu, Appl. Phys. B, 2007, 86: 177
18. J. W. Shi, X. D. Chen, M. Ouyang, J. Liu, and D. H. Liu, Appl. Opt., 2009, 48 (to be published)
19. M. J. Damzen, V. I. Vlad, V. Babin, A. Mocofanescu, Stimulated Brillouin Scattering: Fundamentals and Applications, Bristol: IOP Publishing, 2003
20. R. W. Boyd, Nonlinear Optics, 3rd Ed., Chapter 9, New York: Academic Press, 2008
21. Y. R. Shen, Nonlinear Optics, Chapter 11, New York: John Willey & Sons, 1984
22. J. H. Bai, J. Liu, Y. Huang, Y. N. Liu, L. Sun, D. H. Liu,

and E. S. Fry, Appl. Opt., 2007, 46: 6804
23. N. G. Jerlov, Marine Optics, Chapter 3.3, Elsevier Oceanography Series 14, Amsterdam: Elsvier Scientific Publishing Company, 1976
24. M. R. Querry, P. G. Cary, and R. C. Waring, Appl. Opt., 1978, 17: 3587
25. F. M. Sogandandares and E. S. Fry, Appl. Opt., 1997, 36: 8699
26. R. M. Pope and E. S. Fry, Appl. Opt., 1997, 36: 8710
27. S. A. Sullivan, J. Opt. Soc. Am, 1963, 53: 962
28. G. Rivoire and D. D. Wang, J. Chem. Phys., 1993, 99: 9460
29. H. Su, S. H. Tang, and Y. Q. Qin, Opt. Commun., 2004, 242: 649
30. A. D. Kudryavtseva and N. V. Tcherniega, Journal of Russian Laser Research, 2002, 23: 288
31. D'yakov and E. Yu, J ETP Lett., 1970, 11: 243
32. P. Narum, M. D. Skeldom, and W. Boyd, IEEE J. Quantum Electron., 1986, 22: 2161
33. J. H. Bai, J. W. Shi, M. Ouyang, X. D. Chen, W. P. Gong, H. M. Jing, J. Liu, and D. H. Liu, Opt. Lett., 2008, 33: 1539
34. J. Shi, X. Chen, M. Ouyang, J. Liu, and D. H. Liu, Appl. Phys. B, 2009, 95: 657
35. H. J. Eichler I, R. Konig, H. J. Piitzold, and J. Schwartz, Appl. Phys. B, 1995, 61: 73
36. G. Cook and K. D. Ridley, Opt. Commun., 1996, 130: 192
37. Y. S. Kuo, K. Choi, and J. K. Mclver, Opt. Commun., 1991, 80: 233
38. N. M. Kroll, J. Appl. Phys., 1965, 36: 34
39. D. T. Hon, Opt. Lett., 1980, 5: 516
40. N. Naftali, R. M. J. Bemair, P. Idit, and Y. Ammon, Appl. Opt., 2002, 41: 3576
41. T. Shimizu, K. Nakajima, K. Shiraki, K. Ieda, and I. Sankawa, Optical Fiber Technology, 2008, 14: 10
42. T. Michael, B. Duignan, J. Feldman, and W. T. Whitney, J. Opt. Soc. Am. B, 1992, 9: 548
43. K. O. Hill, B. S. Kawasaki, and D. C. Johnson, Appl. Phys. Lett., 1976, 28: 608
44. J. W. Shi, M. Ouyang, X. D. Chen, B. Liu, Y. X. Xu, H. M. Jing, and D. H. Liu, Opt. Lett., 2009, 34: 977
45. D. H. Liu, J. W. Shi, M. Ouyang, X. D. Chen, J. Liu, and X. D. He, Phys. Rev. A, 2009, 80: 033808
46. D. Wang, R. Barille, and G. Riviore, J. Opt. Soc. Am. B, 1997, 14: 2584
47. N. Tchemiega, A. Sokolovskaia, A. D. Kudriavtsva, R. Barille, and G. Riviore, Opt. Commun., 2000, 181: 197
48. D. C. Jones, M. S. Mangir, D. A. Rockwell, and J. O. White, J. Opt. Soc. Am. B, 1990, 7: 2090
49. M. Maier, W. Kaiser, and J. A. Giordmaine, Phys. Rev. Lett., 1966, 17: 1275
50. M. Maier, W. Kaiser, and J. A. Giordmaine, Phys. Rev., 1969, 177: 580
51. D. Pohl, M. Maier, and W. Kaiser, Phys. Rev. Lett., 1968, 20: 366
52. R. W. Minck, E. E. Hagenlocker, and W. G. Rado, J. Appl. Phys., 1967, 38: 2254
53. X. Hua, J. Leng, H. Yang, G. Sha, and C. Zhang, Appl. Phys. B, 2005, 81: 525
54. W. R. Trutna, Y. Kwanpark, and R. L. Byer, IEEE. J. Quant. Electron., 1979, 15: 648
55. J. Z. Zhang, G. Chen, and R. K. Chang, J. Opt. Soc. Am. B, 1990, 7: 108
56. M. J. Weber, Handbook of Laser Science and Technology, Supplement 2: Optical Materials, CRC Press, 1994